JOURNAL OF PROTEOMICS 75 (2012) 5822–5847

Available online at www.sciencedirect.com

SciVerse ScienceDirect

www.elsevier.com/locate/jprot

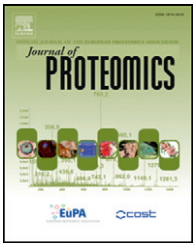

Proteomic analysis of proteins responsible for the development of doxorubicin resistance in human uterine cancer cells

Szu-Ting Lin[a,b], *Hsiu-Chuan Chou*[c], *Shing-Jyh Chang*[d,e], *Yi-Wen Chen*[a,b], *Ping-Chiang Lyu*[a,b], *Wen-Ching Wang*[f,g], *Margaret Dah-Tsyr Chang*[f,g], *Hong-Lin Chan*[a,b,*]

[a]*Department of Medical Science, National Tsing Hua University, Hsinchu, Taiwan*
[b]*Institute of Bioinformatics and Structural Biology, National Tsing Hua University, Hsinchu, Taiwan*
[c]*Department of Applied Science, National Hsinchu University of Education, Hsinchu, Taiwan*
[d]*Department of Obstetrics and Gynecology, MacKay Memorial Hospital Hsinchu Branch, Hsinchu, Taiwan*
[e]*Department of Nursing, Yuanpei University, Hsinchu, Taiwan*
[f]*Institute of Molecular and Cellular Biology, National Tsing Hua University, Hsinchu, Taiwan*
[g]*Department of Medical Science, National Tsing Hua University, Hsinchu, Taiwan*

ARTICLE INFO

Article history:
Received 31 March 2012
Accepted 20 July 2012

Keywords:
Proteomics
DIGE
MALDI-TOF
Doxorubicin
Resistance
Uterine cancer

ABSTRACT

Drug resistance is a common cause of failure in cancer chemotherapy treatments. In this study, we used a pair of uterine sarcoma cancer lines, MES-SA, and the doxorubicin-resistant MES-SA/Dx5 as a model system to examine resistance-dependent cellular responses and to identify potential therapeutic targets. We used two-dimensional differential gel electrophoresis (2D-DIGE) and matrix-assisted laser desorption ionization time-of-flight mass spectrometry (MALDI-TOF/TOF MS) to examine the global protein expression changes induced by doxorubicin treatment and doxorubicin resistance. A proteomic study revealed that doxorubicin-exposure altered the expression of 87 proteins in MES-SA cells, while no significant response occurred in similarly treated MES-SA/Dx5 cells, associating these proteins with drug specific resistance. By contrast, 37 proteins showed differential expression between MES-SA and MES-SA/Dx5, indicating baseline resistance. Further studies have used RNA interference, cell viability analysis, and analysis of apoptosis against asparagine synthetase (ASNS) and membrane-associated progesterone receptor component 1 (mPR) proteins, to monitor and evaluate their potency on the formation of doxorubicin resistance. The proteomic approach allowed us to identify numerous proteins, including ASNS and mPR, involved in various drug-resistance-forming mechanisms. Our results provide useful diagnostic markers and therapeutic candidates for the treatment of doxorubicin-resistant uterine cancer.

Abbreviations: 1-DE, one-dimensional gel electrophoresis; 2-DE, two-dimensional gel electrophoresis; Ab, antibody; CCB, colloidal coomassie blue; CHAPS, 3-[(3-cholamidopropyl)-dimethylammonio]-1-propanesulfonate); ddH_2O, double deionized water; DIGE, differential gel electrophoresis; DTT, dithiothreitol; FCS, fetal calf serum; MALDI-TOF MS, matrix assisted laser desorption ionization-time of flight mass spectrometry; NP-40, Nonidet P-40; TFA, trifluoroacetic acid

* *Corresponding author at:* Institute of Bioinformatics and Structural Biology and Department of Medical Sciences, National Tsing Hua University, No. 101, Kuang-Fu Rd. Sec. 2, Hsin-chu, 30013, Taiwan. Tel.: +886 3 5742476; fax: +886 3 5715934.
E-mail address: hlchan@life.nthu.edu.tw (H.-L. Chan).

1874-3919/$ – see front matter © 2012 Elsevier B.V. All rights reserved.
http://dx.doi.org/10.1016/j.jprot.2012.07.047

1. Introduction

Drug resistance reduces the effectiveness of medications used in the treatment of diseases such as cancer. In clinical practice, resistance becomes a serious problem when the concentrations of anticancer compounds at dosages needed to kill tumor cells, reach toxic levels. Biological processes associated with drug resistance have been described, and include the enhanced activities of membrane-embedded drug efflux transporter molecules such as adenosine triphosphate binding cassette (ABC)-transporters, the alteration of drug targeting molecules that repair pathways, and the modulation of cellular signal transduction pathways that lead to cell death [1].

Doxorubicin is an anticancer drug used in the treatment of a wide range of cancers, including lung cancer, breast cancer, and many other carcinoma types [2–4]. Doxorubicin's precise mechanism of action is complex; it interacts with DNA by intercalation into DNA molecules from where it may inhibit the synthesis of DNA, RNA, and proteins. Doxorubicin resistance has been widely reported in reports of cancer research into leukemia, osteosarcoma, breast cancer, lung cancer, and uterine cancer [5–9], and is a major obstacle to the successful treatment of cancer patients receiving chemotherapy.

Two-dimensional electrophoresis (2-DE) is a key technique used in the profiling of thousands of proteins in biological samples; it plays a complementary role to LC/MS-based proteomic analysis [10]. However, a reliable quantitative comparison between gels and gel-to-gel variations is a challenge for 2-DE analysis. The introduction of 2D-DIGE was a significant improvement in gel-based protein quantitation and detection; the method can co-detect numerous samples that are present in the same 2-DE. 2D-DIGE minimizes gel-to-gel variations, and compares the relative amounts of protein features across different gels by using an internal fluorescent standard. Moreover, the technique offers the advantages of a broader dynamic range, increased sensitivity, and greater reproducibility than traditional 2-DE does. 2D-DIGE innovative technology relies on the pre-labeling of protein samples with fluorescent dyes (Cy2, Cy3, and Cy5) before commencing electrophoresis. Each dye type has a unique fluorescence wavelength, allowing the simultaneous separation of multiple samples, each containing an internal standard. The standard, which is a pool of an equal quantity of the experimental protein samples, provides accurate normalization data and increases the statistical confidence for relative quantitation among different gels [11–13].

The aims of this investigation were to conduct an in vitro investigation into doxorubicin-resistance mechanisms in uterine cancer using proteomic strategies, to increase our understanding of the molecular processes involved, and to identify potential resistance biomarkers with possible diagnostic or therapeutic applications. Thus, we selected a pair of uterine sarcoma cancer lines, MES-SA, and its doxorubicin-resistant partner MES-SA/Dx5 as a model system to examine resistance-dependent cellular protein expression. The literature also contains reports of studies that used RNA interference against selected identified proteins, ASNS, and membrane-associated progesterone receptor component 1 (mPR) to monitor and evaluate their potency against doxorubicin resistance.

2. Materials and methods

2.1. Chemicals and reagents

Generic chemicals were purchased from Sigma-Aldrich (St. Louis, USA), and the reagents for 2D-DIGE were purchased from GE Healthcare (Uppsala, Sweden). All the chemicals and biochemicals used in this study were of analytical grade. All Western blot and ELISA used with primary antibodies were purchased from Genetex (Hsinchu, Taiwan) and anti-mouse, and anti-rabbit secondary antibodies were purchased from GE Healthcare (Uppsala, Sweden).

2.2. Cell lines and cell cultures

The uterine sarcoma cancer line MES-SA and its doxorubicin resistance line MES-SA/Dx5 were both purchased from the American Type Culture Collection (ATCC), Manassas, VA [14,15]. Cells were cultured in McCoy's 5a modified medium containing 10% fetal bovine serum, L-glutamine (2 mM), streptomycin (100 μg/mL), penicillin (100 IU/mL) (all from Gibco-Invitrogen Corp., UK) and maintained without / with 0.4 μM doxorubicin, respectively. All cells were incubated at 37 °C in a humidified atmosphere containing 5% CO_2.

2.3. MTT cell viability assay

MES-SA and MES-SA/Dx5 cells (5000 cells/well) growing exponentially were seeded into 96-well plates. The culture cells were incubated for 24 h before treatment with indicative concentrations of doxorubicin for 48 h and untreated as control. After removal of the medium, 100 μL of MTT working solution (1 mg/mL) (Sigma) was added into each well, followed by a further incubation at 37 °C in 5% CO_2 for 4 h. The supernatant was carefully removed followed by added 100 μL of DMSO to each well and shaken for 15 min. The absorbance of samples was measured at a wavelength of 540 nm in a multi-well plate reader. Values were normalized against the untreated samples and were averaged from 8 independent measurements.

2.4. Sample preparation for proteomic analysis

Cells grow in ~80% confluence and treated with/without 0.1 μM doxorubicin for 48 h. For total cellular protein analysis, both MES-SA and MES-SA/Dx5 cells were washed in chilled 0.5×PBS and scraped in 2-DE lysis buffer containing 4% w/v CHAPS, 7 M urea, 2 M thiourea, 10 mM Tris–HCl, pH 8.3, 1 mM EDTA. Lysates were homogenized by passage through a 25-gauge needle at least ten times, insoluble material was removed by centrifugation at 13,000 rpm for 30 min at 4 °C, and protein concentrations were determined using coomassie protein assay reagent (BioRad).

2.5. 2D-DIGE and gel image analysis

Quantified protein samples were labeled with N-hydroxy succinimidyl ester-derivatives of the cyanine dyes Cy2, Cy3 and Cy5. In brief, 150 μg of protein sample was minimally labeled with 375 pmol of either Cy3 or Cy5 for comparison on the same 2-DE. In order to facilitate image matching and cross-gel statistical comparison, a pool of all samples in each condition was also prepared and labeled with Cy2 at a molar ratio of 2.5 pmol per μg of protein as an internal standard for all gels. Hence, the triplicate protein samples and the internal standard could be run and quantified on multiple 2-DE. The labeling reactions were performed in the dark on ice for 30 min and then dyes were quenched with a 20-fold molar ratio excess of free L-lysine for 10 min. The differentially Cy3- and Cy5-labeled samples were mixed with the Cy2-labeled internal standard and reduced with dithiothreitol for 10 min. IPG buffer, pH 3–10 nonlinear (2% (v/v), GE Healthcare) was added and the final volume was adjusted to 400 μL with 2D-lysis buffer for rehydration. The rehydration process was performed with immobilized non-linear pH gradient (IPG) strips (pH 3–10, 24 cm) which were later rehydrated by CyDye-labeled samples in the dark at room temperature at least 12 h. Isoelectric focusing was then performed using a Multiphor II apparatus (GE Healthcare) for a total of 62.5 kV-h at 20 °C. Strips were equilibrated in 6 M urea, 30% (v/v) glycerol, 1% SDS (w/v), 100 mM Tris–HCl (pH 8.8), 65 mM dithiothreitol for 15 min and then in the same buffer containing 240 mM iodoacetamide for another 15 min. The equilibrated IPG strips were transferred onto 26×20-cm 12.5% polyacrylamide gels cast between low fluorescent glass plates. The strips were overlaid with 0.5% (w/v) low melting point agarose in a running buffer containing bromophenol blue. The gels were run in an Ettan Twelve gel tank (GE Healthcare) at 4 W per gel at 10 °C until the dye front had completely run off the bottom of the gels. Afterward, the fluorescence 2-DE gels were scanned directly between the low fluorescent glass plates using an Ettan DIGE Imager (GE Healthcare). This imager is a charge-coupled device-based instrument that enables scanning at different wavelengths for Cy2-, Cy3-, and Cy5-labeled samples. Gel analysis was performed using DeCyder 2-D Differential Analysis Software v7.0 (GE Healthcare) to detect, normalize and quantify the protein features in the images. Features detected from non-protein sources (e.g. dust particles and dirty backgrounds) were filtered out. Spots displaying in a ≧1.5 average-fold increase or decrease in abundance with a p-value<0.05 were selected for protein identification.

2.6. Protein staining

Colloidal coomassie blue G-250 staining was used to visualize CyDye-labeled protein features in 2-DE. Bonded gels were fixed in 30% v/v ethanol, 2% v/v phosphoric acid overnight, washed three times for each 30 min with ddH_2O and then incubated in 34% v/v methanol, 17% w/v ammonium sulphate, 3% v/v phosphoric acid for 1 h, prior to adding 0.5 g/L coomassie blue G-250. The gels were left to stain for 3–5 days. No destaining step was required. The stained gels were imaged on an ImageScanner III densitometer (GE Healthcare), which processed the gel images as .tif files.

2.7. In-gel digestion

Excised post-stained gel pieces were washed three times in 50% acetonitrile, and then dried in a SpeedVac for 20 min, reduced with 10 mM dithiothreitol in 5 mM ammonium bicarbonate pH 8.0 (ammonium bicarbonate) for 45 min at 56 °C and then alkylated with 50 mM iodoacetamide in 5 mM ammonium bicarbonate for 1 h at room temperature in the dark. The gel pieces were washed two times in 50% acetonitrile and vacuum-dried before reswelling with 50 ng of modified trypsin (Promega) in 5 mM ammonium bicarbonate. The pieces were overlaid with 10 μL of 5 mM ammonium bicarbonate and trypsinized for 16 h at 37 °C. Supernatants were collected, peptides were further extracted twice with 5% trifluoroacetic acid in 50% acetonitrile and the supernatants were pooled. Peptide extracts were vacuum-dried, resuspended in 5 μL ddH_2O, and stored at −20 °C prior to MS analysis.

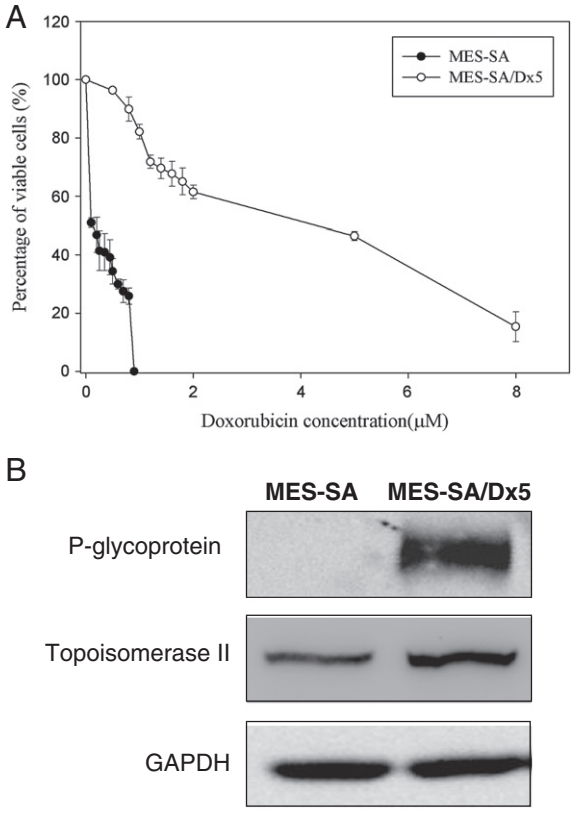

Fig. 1 – Dose-dependent kinetics of doxorubicin-induced loss of cell viability and increased expression of P-glycoprotein and topoisomerase 2 in MES-SA and MES-SA/Dx5 cells. (A) MES-SA and MES-SA/Dx5 cells grown overnight were treated with a range of doses of doxorubicin and cell viability was determined by MTT assay. (B) Expression of P-glycoprotein and topoisomerase 2 in MES-SA and MES-SA/Dx5 cells were monitored by immunoblotting.

2.8. *Protein identification by MALDI-TOF/TOF MS*

For protein identification, extracted peptides were subjected to peptide mass fingerprinting (PMF) using MALDI-TOF MS. Briefly, 0.5 μL of trypsin digested protein sample was mixed with 0.5 μL of a matrix solution containing α-cyano-4-hydroxycinammic acid at a concentration of 1 mg/mL of 50% ACN/0.1% TFA (v/v), spotted onto an anchorchip target plate (Bruker Daltonics) and dried. The peptide mass fingerprints were acquired using an Autoflex III mass spectrometer

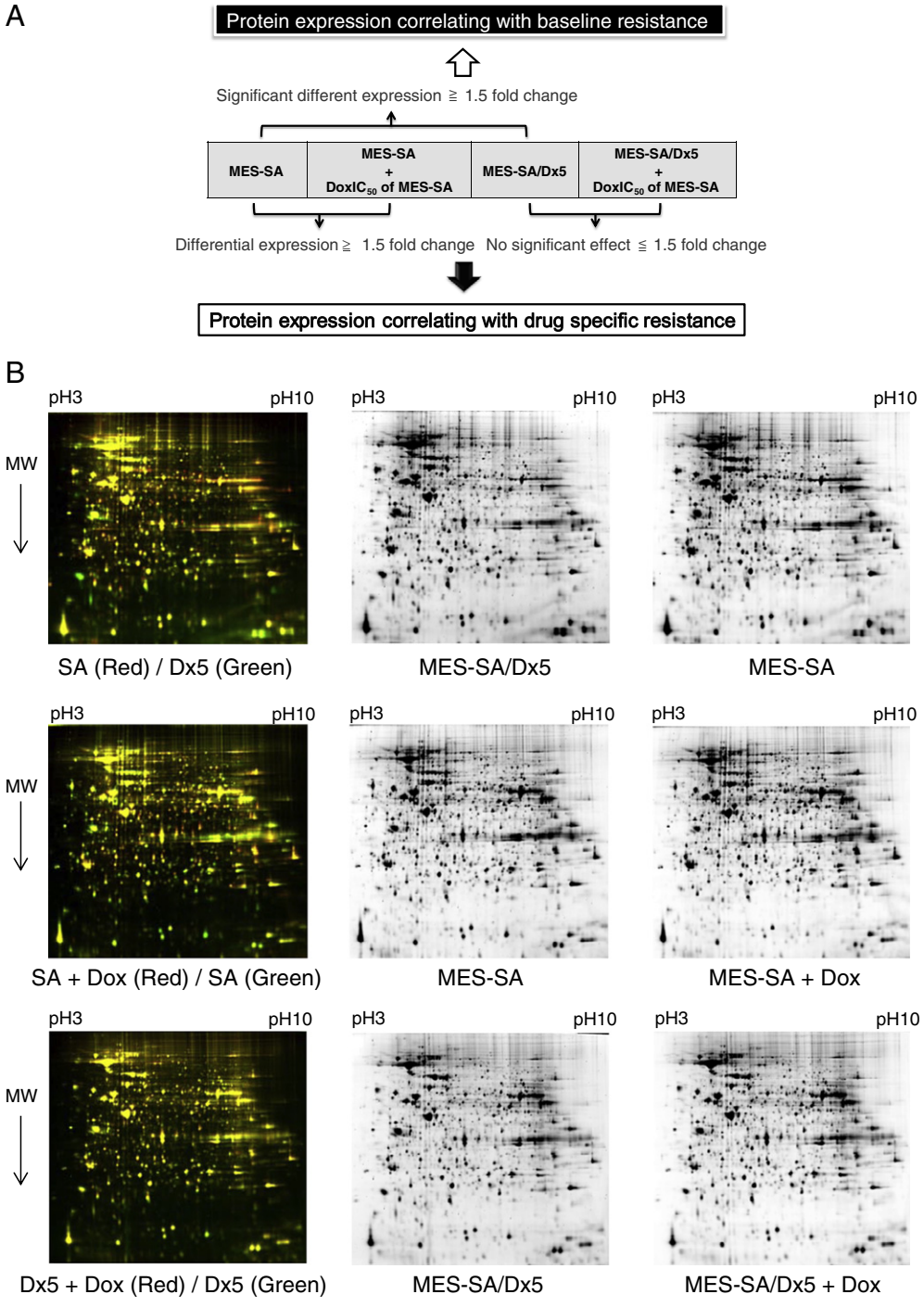

Fig. 2 – Proteomic comparison across MES-SA and MES-SA/Dx5 treated with/without doxorubicin. (A) Schematic representation of the 2D-DIGE workflow to monitor the differentially expressed proteins correlated to baseline resistance and doxorubicin specific resistance in uterine cancer. (B) 2D-DIGE images of MES-SA and MES-SA/Dx5 treated with IC_{50} concentration of doxorubicin of MES-SA or left untreated.

Table 1 – Alphabetical list of identified differentially expressed proteins between doxorubicin sensitive uterine cancer cells (MES-SA) and doxorubicin resistant uterine cancer cells (MES-SA/Dx5) obtained after 2D-DIGE coupled with MALDI-TOF mass spectrometry analysis. [a] Average ratio of differential expression (≥1.5-fold increase or decrease) between doxorubicin resistant uterine cancer cells (MES-SA/Dx5) and doxorubicin sensitive uterine cancer cells (MES-SA). [b] Average ratio of differential expression (≥1.5-fold increase or decrease) between 0.1 μM doxorubicin-treated and untreated MES-SA cells. [c] Average ratio of differential expression (≥1.5-fold increase or decrease) between 0.1 μM doxorubicin-treated and untreated MES-SA/Dx5 cells. Gray shaded cells indicate proteins where the changes between 0.1 μM doxorubicin-treated and untreated MES-SA cells are significantly greater than the changes between 0.1 μM doxorubicin-treated and untreated MES-SA/Dx5 cells. [d] These proteins have been identified by both MALDI-TOF MS and MALDI-TOF/TOF MS. The parameters (sequence coverages, MASCOT values, matched peptide numbers and matched peptide sequences) shown in brackets are obtained from MALDI-TOF/TOF MS sequence analysis. e. In MS analysis, we listed top 2 score peptide sequences in the matched peptide column. In MS/MS analysis, we listed the MS/MS-sequenced peptide with bracket in the matched peptide column.

Spot No.	swiss-prot No.	Gene name	Protein name	pI	MW	No. Match. Peptides	Cov. (%)	Score	Subcellular location	Functional ontology	matched peptides[e]	Dx5 / SA[a]	T-test	SA + Do x 0.1μ M / SA[b]	T-test	Dx5 + Dox 0.1 μ M / Dx5[c]	T-test
1457	P62258	YWHAE	14-3-3 protein epsilon	4.63	29326	10/22	27%	77/56	Cytoplasm	Signal transduction	MDDREDLVYQ AK DSTLIMQLLR	1.2	0.002	1.73	0.00089	1.05	0.2
1499	P61981	YWHAG	14-3-3 protein gamma	4.8	28456	12/38	27%	80/56	Cytoplasm	Signal transduction	MVDREQLVQK YLAEVATGEK	1.22	0.0093	1.86	0.0016	1	0.95
1748	P27348	YWHAQ	14-3-3 protein theta	4.68	28032	12/31	36%	107/56	Cytoplasm	Signal transduction	YLAEVACGDDR DSTLIMQLLR	-1.1	0.058	1.52	0.0029	1.26	0.012
1521	P63104	YWHAZ	14-3-3 protein zeta/delta	4.73	27899	11/29	31%	89/56	Cytoplasm	Signal transduction	FLIPNASQAESK DSTLIMQLLR	-1.45	0.0011	1.69	0.0031	1.16	0.085
935	P43686	PSMC4	26S protease regulatory subunit 6B	5.09	57451	8/21	18%	70/56	Cytoplasm	Protein degradation	EFLHAQEEVKR AVAHHTTAAFI R	-1.1	0.099	-1.6	0.00058	-1.15	0.062
1015	P62333	PSMC6	26S protease regulatory subunit S10B/Proteasome 26S subunit ATPase 6/PSMC6	7.1	44430	8/30	22%	58/56	Cytoplasm	Protein degradation	KIHIDLPNEQAR LSDGFNGADLR	-1.32	0.0094	-1.72	0.017	-1.09	0.25
955	O00231	PSMD11	26S proteasome non-ATPase regulatory subunit 11	6.08	47719	8/21	19%	75/56	Proteasome	Protein degradation	AAAAVVEFQR YAGRQTEALK	-1.2	0.025	1.5	0.0043	1.22	0.0058
815	Q16401	PSMD5	26S proteasome non-ATPase regulatory subunit 5	5.35	56560	8/21	18%	79/56	Proteasome	Protein degradation	ALHSVLQAVPL NELR TIAEIFGNPNYL R	-1.3	0.014	1.55	0.0004	1.26	0.026
1519	P48556	PSMD8	26S proteasome non-ATPase regulatory subunit 8/p31	6.85	30157	6/23	15%	70/56	Proteasome	Protein degradation	QVIEYAR VAEFHTELER	-1.69	0.0046	1.29	0.018	1.42	0.04
1090	P08865	RPSA	40S ribosomal protein SA / Multidrug resistance-associated protein MGr1-Ag / Laminin receptor 1	4.79	32947	7/19	31%	92/56	Membrane	Cell adhesion	SDGIYIINLKR FTPGTFTNQIQA AFR	-1	0.92	1.6	0.0044	1.19	0.069
1514	O95336	PGLS	6-phosphogluconolactonase	5.7	27815	6/11	34%	119/56	Cytoplasm	Metabolism	WTLGFCDER VTLTLPVLNAA R	1.23	0.00071	-1.76	0.0086	-1.13	0.086
1710	Q96IU4	ABHD14B	Abhydrolase domain-containing protein 14B/ABHD14B	5.94	22446	6/27	32%	86/56	Cytoplasm	Gene regulation	FSVLLLHGIR AVAIDLPGLGHS K	1.08	0.0071	-1.57	0.00048	-1.17	0.0038
1529	Q7M4N6	ANP32A	Acidic leucine-rich nuclear phosphoprotein 32 family member A/Potent heat-stable protein phosphatase 2A inhibitor I1PP2A/ANP32A /Lanp	3.99	28682	4/9	15%	58/56	Nucleus	Signal transduction	RIHLELR LLPQLTYLDGY DR	1.03	0.25	-1.74	0.017	-1.21	0.041
905	P61158	ACTR3	Actin-related protein 3	5.61	47797	7/19	17%	80/56	Cytoplasm	Cytoskeleton	EFSIDVGYER DYEEIGPSICR	-1.69	0.000038	1.17	0.0058	-1.02	0.66

1657	P07741	APRT	Adenine phosphoribosyltransferase / APRT[d]	5.78	19766	4/6 (1/1)	26% (7%)	69/56 (60/29)	Cytoplasm	Biosynthesis	ADSELQLVEQR IDYIAGLDSR (SFPDFPTPGVV FR)	1.32	0.035	-2.03	0.00012	-1.1	0.34
248	Q96FA0	AARS	Alanyl-tRNA synthetase, cytoplasmic	5.34	107484	7/13	8%	62/56	Cytoplasm	Biosynthesis	FIDFFKR GTGARPYTGK	1.25	0.0041	-1.52	0.00027	6	0.049
877	P22712	ENO1	Alpha-enolase	7.01	47481	8/27	19%	68/56	Cytoplasm	Metabolism	YISPDQLADLY K IGAEVYHNLK	-1.14	0.044	-1.9	0.00011	-1.21	0.033
1415	P09525	ANXA4	Annexin A	5.84	36088	10/25	34%	125/56	Cytoplasm	Signal transduction	ISQTYQQQYGR DEGNYLDDALV R	1.37	0.0017	1.98	0.00014	-1.1 1.25	0.001
1399	P08758	ANXA5	Annexin A5	4.94	35971	8/20	27%	88/56	Membrane	Signal transduction	SEIDLFNIR NFATSLYSMIK	-1.9	0.00002	1.63	0.00032	1.22	0.0032
973	P20073	ANXA7	Annexin A7	5.52	52991	7/20	15%	64/56	Membrane	Signal transduction	CYQSEFGR LYQAGEGR	-1.35	0.0008	1.67	0.0014	1.25	0.047
1578	Q5U0H4	BCL2L2	Apoptosis regulator Bcl-W	5.82	20875	4/8	26%	66/56	Mitochondrion	Signal transduction	ATPASAPDTR EGNWASVR	1.31	0.014	-1.82	0.00024	-1.28	0.031
674	P08243	ASNS	Asparagine synthetase [glutamine-hydrolyzing]	6.39	64899	8/42	15%	71/56	Cytoplasm	Biosynthesis	DTYGVRPLFK LAVVDPLFGMQ PIR	4.12	0.00005	1.19	0.49	1.03	0.81
670	P08243	ASNS	Asparagine synthetase [glutamine-hydrolyzing]	6.39	64899	9/17	13%	73/56	Cytoplasm	Biosynthesis	DTYGVRPLFK TKEGYYYR	3.41	0.056	1.31	0.53	1.16	0.48
1048	P17174	GOT1	Aspartate aminotransferase	6.52	46451	8/26	24%	81/56	Cytoplasm	Metabolism	ITWSNPPAQGA R HIYLLPSGR	1.15	0.13	1.57	0.003	1.16	0.012
1739	P31939	ATIC	Bifunctional purine biosynthesis protein PURH/IMP cyclohydrolase	6.27	65089	8/15	17%	89/56	Cytoplasm	Biosynthesis	TLHPAVHAGIL AR ANYWWLR	-1.75	0.000069	-1.32	0.011	-1.01	0.86
1743	O43852	CALU	Calumenin	4.47	37198	6/16	19%	62/56	ER	Metabolism	WIYEDVER TEREQFVEFR	3	0.0069	-1.87	0.044	-1.36	0.042
157	Q8N6T1	CSTF2T	Cleavage stimulation factor 64 kDa subunit, tau variant	6.79	64624	6/18	14%	59/56	Nucleus	Gene regulation	IMDPEIALK GPMIDQR	1.8	0.00015	-1.07	0.15	-1.01	0.83
1680	P23528	CFL1	Cofilin-1[d]	8.22	18719	6/13 (1/1)	26% (6%)	64/56 (49/29)	Cytoplasm	Cytoskeleton	YALYDATYETK MLPDKDCR (YALYDATYETK)	1.11	0.11	-4.43	0.0002	-1.65	0.0045
1077	Q561W7	COPS4	COP9 signalosome complex subunit 4	5.57	46525	8/17	23%	89/56	Nucleus	Signal transduction	VISFEEQVASIR TIVHESERLEAL K LAVEALSSLDG	-1.26	0.0015	1.5	0.0045	1.06	0.0092

Spot No.	swiss-prot No.	Gene name	Protein name	pI	MW	No. Match. Peptides	Cov. (%)	Score	Subcellular location	Functional ontology	matched peptides[e]	Dx5 / SA[a]	T-test	SA + Do x 0.1μ M / SA[b]	T-test	Dx5 + Dox 0.1 μ M / Dx5[c]	T-test
102	P12277	CKB	Creatine kinase B-type	5.34	42902	10/35	33%	113/56	Cytoplasm	Metabolism	DL GTGGVDTAAV GGV	2.3	0.000024	1.16	0.12	-1.1	0.019
1410	P53701	HCCS	Cytochrome c-type heme lyase	6.25	30981	8/23	29%	100/56	Mitochondrion	Electron transport	TYSVPAHQER SWMGYELPFDR	1.93	0.036	-1.15	0.43	-1.17	0.22
1484	Q6IBH9	EEF1B2	Elongation factor 1-beta	4.5	24919	4/16	15%	56/56	Cytoplasm	Biosynthesis	WYNHIK LVPVGYGIK	-1.07	0.16	-1.85	0.004	-1.22	0.0064
1335	P29692	EEF1D	Elongation factor 1-delta	4.9	31417	9/25	34%	98/56	Cytoplasm	Biosynthesis	ATNFLAHEK QENGASVILR	-1.15	0.037	-1.52	0.016	-1.3	0.022
1505	P30040	ERP29	Endoplasmic reticulum resident protein 29/ ERp29	6.77	29032	11/25	35%	119/56	ER	Protein folding	ESYPVFYLFR ILDQGEDFPASE MTR	1.07	0.029	-1.94	0.0012	-1.23	0.0012
1513	P30040	ERP29	Endoplasmic reticulum resident protein 29/ ERp29	6.77	29032	8/16	28%	92/56	ER	Protein folding	ESYPVFYLFR ILDQGEDFPASE MTR	1.27	0.0016	-1.61	0.011	-1.21	0.0036
967	B2R6L8	EIF4A1	Eukaryotic initiation factor 4A-I/eIF-4A-I	5.32	46353	11/33	23%	93/56	Cytoplasm	Translational regulation	ATQALVLAPTR QFYINVER	1	0.98	1.54	0.00041	1.35	0.0096
1199	P05198	EIF2S1	Eukaryotic translation initiation factor 2 subunit 1	5.02	36374	6/18	19%	60/56	Cytoplasm	Protein synthesis	DEQLESLFQR TEGLSVLSQAM AVIKEK	-1.01	0.73	1.58	0.0014	1.36	0.0013
1689	P63241	EIF5A	Eukaryotic translation initiation factor 5A-1	5.08	17049	7/20	58%	86/56	Cytoplasm	Biosynthesis	KYEDICPSTHN MDVPNIK EDLRLPEGDLG K	1.13	0.16	-1.96	0.014	-1.41	0.01
1746	P47756	CAPZB	F-actin-capping protein subunit beta	5.36	31616	9/23	29%	95/56	Cytoplasm	Cytoskeletal organization	SDQQLDCALDL MR KLEVEANNAFD QYR	1.06	0.55	1.69	0.0009	1.12	0.21
1161	P04075	ALDOA	Fructose-bisphosphate aldolase A	8.3	39851	6/13	20%	76/56	Cytoplasm	Metabolism	IGEHTPSALAIM ENANVLAR CPLLKPWALTF SYGR	1.17	0.064	-1.56	0.0039	-1.14	0.11
982	P07954	FH	Fumarate hydratase, mitochondrial	8.85	54773	7/15	15%	78/56	Mitochondrion	Metabolism	VPNDKYYGAQ TVR	1.17	0.3	1.71	0.0066	1	0.94

1709	P51570	GALK1	Galactokinase / Galactose kinase	6.04	42702	7/28	15%	87/56	Cytoplasm	Metabolism	IPVHPNDHVNK QPQVAELLAEA R	1.45	0.0074	-1.7	0.00056	-1.15	0.16
710	P11413	G6PD	Glucose-6-phosphate 1-dehydrogenase	6.39	59675	7/29	16%	79/56	Cytoplasm	Metabolism	LAVLITNSNVR IIVEKPFGR GGYFDEFGIIR	-2.15	1.7E-06	-1.06	0.28	-1	0.79
1474	Q7Z3T2	GSTO1	Glutathione S-transferase omega-1[d]	5.42	27833	6/15 (1/1)	24% (5%)	69/56 (43/29)	Cytoplasm	Redox regulation	GSAPPGPVPEGS IR VPSLVGSFIR (GSAPPGPVPEG SIR)	1.18	0.00019	-2.08	0.000002	-1.03	0.076
484	P49915	GMPS	GMP synthase [glutamine-hydrolyzing]/GMP synthetase	6.42	77408	6/13	11%	58/56	Cytoplasm	Biosynthesis	DFHKDEVR VVYIFGPPVK	1	0.95	-1.57	0.00023	-1.13	0.054
1644	Q9HAV7	GRPEL1	GrpE protein homolog 1, mitochondrial	8.24	24492	4/12	21%	62/56		Protein Mitochondrion folding	LYGIQAFCK TLRPALVGVVK	1.12	0.078	-1.68	0.0095	-1.24	0.032
1429	P63244	GNB2L1	Guanine nucleotide-binding protein subunit beta-2-like 1 / Receptor of activated protein kinase C 1 / RACK1	7.6	35511	7/26	28%	72/56	Membrane	Signal transduction	DETNYGIPQR VWQVTIGTR	1.14	0.072	2.36	0.001	1.04	0.51
549	P11142	HSPA8	Heat shock cognate 71 kDa protein	5.37	71082	7/14	16%	107/56	Cytoplasm	Protein folding	DAGTIAGLNVL R FEELNADLFR	1.15	0.41	-1.95	0.015	-1.05	0.8
545	P11142	HSPA8	Heat shock cognate 71 kDa protein	5.37	71082	7/22	16%	88/56	Cytoplasm	Protein folding	DAGTIAGLNVL R ARFEELNADLF R	1.07	0.76	-1.94	0.00086	-1.21	0.31
550	P11142	HSPA8	Heat shock cognate 71 kDa protein	5.37	71082	8/23	18%	114/56	Cytoplasm	Protein folding	DAGTIAGLNVL R FEELNADLFR	1.31	0.026	-1.92	0.0037	-1.22	0.05
244	Q92598	HSPH1	Heat shock protein 105 kDa	5.28	97716	6/17	9%	64/56	Cytoplasm	Protein folding	FICEQDHQNFLR LVEHFCAEFK	1.51	0.00013	-1.33	0.028	-1.07	0.027
1725	P10809	HSPD1	Heat shock protein 60 kDa, mitochondrial	5.7	61187	12/26	27%	116/56	Mitochondrion	Protein folding	TVIIEQSWGSPK CEFQDAYVLLS EK	1.06	0.093	-1.79	0.042	-1.14	0.04
1738	Q12931	TRAP1	Heat shock protein 75 kDa / TNFR-associated protein 1/TRAP1	8.3	80345	6/20	10%	66/56	Mitochondrion	Protein folding	YVAQAHDKPR NIYYLCAPNR	-1.24	0.0065	2.02	0.00047	1.2	0.046
500	Q12931	TRAP1	Heat shock protein 75 kDa / TNFR-associated protein 1/TRAP1	8.3	80345	6/12	10%	82/56	Mitochondrion	Protein folding	EWQHEEFYR FFEDYGLFMR	-1.17	0.028	2.05	0.0003	1.08	0.081

Spot No.	swiss-prot No.	Gene name	Protein name	pI	MW	No. Match.	Cov. (%)	Score	Subcellular location	Functional ontology	matched peptides[e]	Dx5 / SA[a]	T-test	SA + Do x 0.1μ M / SA[b]	T-test	Dx5 + Dox 0.1 μ M / Dx5[c]	T-test
1719	Q6FI47	HSPB1	Heat shock protein beta-1 / Hsp27[d]	5.98	22826	10/31 (1/1)	40% (4%)	107/56 (77/29)	Cytoplasm	Protein folding	LFDQAFGLPR QDEHGYISR (LFDQAFGLPR)	1.41	0.0014	-1.86	0.016	-1.24	0.018
1328	P22626	HNRNP A2B1	Heterogeneous nuclear ribonucleoproteins A2/B1	8.97	37464	6/19	19%	78/56	Nucleus	Gene regulation	NYYEQWGK GGNFGFGDSR	1.07	0.15	-1.79	0.005	-1.24	0.0063
1227	P22626	HNRNP A2B1	Heterogeneous nuclear ribonucleoproteins A2/B1	8.97	37464	7/19	22%	87/56	Nucleus	Gene regulation	GGNFGFGDSR NMGGPYGGGN YGP	1.65	0.0058	-1.57	0.018	-1.2	0.12
1132	Q53EX2	HNRNP C	Heterogeneous nuclear ribonucleoproteins C1/C2	4.95	33707	6/13	16%	66/56	Nucleus	Gene regulation	SDVEAIFSKYGK MYSYPAR	1.34	0.0018	-1.71	0.0058	-1.2	0.014
1129	Q53EX2	HNRNP C	Heterogeneous nuclear ribonucleoproteins C1/C2	4.95	33707	5/19	17%	58/56	Nucleus	Gene regulation	VFIGNLNTLVV K GFAFVQYVNER	1.61	0.00048	-1.5	0.0029	-1.16	0.019
813	Q09028	RBBP4	Histone-binding protein RBBP4	4.74	47911	11/28	23%	109/56	Nucleus	Gene regulation	INHEGEVNR TVALWDLR	1.41	0.00035	-1.6	0.00062	-1.19	0.0098
1050	Q86YM7	HOMER 1	Homer protein homolog 1	5.33	40366	5/11	11%	62/56	Cytoplasm	Cytoskeleton	EEEIER ELQEQR	1.79	0.027	-1.23	0.15	-1.1	0.31
1385	Q15181	PPA1	Inorganic pyrophosphatase / Pyrophosphate phospho-hydrolase	5.54	33095	7/16	25%	80/56	Cytoplasm	Metabolism	AAPFSLEYR YVANLFPYK	1.25	0.00009	-1.87	0.0011	-1.21	0.0003
1726	Q9NVW7	ISYNA1	Inositol-3-phosphate synthase / IPS 1	5.52	57727	5/10	12%	58/56	Cytoplasm	Biosynthesis	VIVLWTANTER YVPYVGDSKR	-3.63	0.0063	-1.24	0.29	1.01	0.95
996	O75874	IDH1	Isocitrate dehydrogenase [NADP] cytoplasmic	6.35	46915	7/15	20%	77/56	Cytoplasm	Metabolism	LVSGWVKPIIIG R TVEAEAAHGTV TR	-1.61	0.00045	-1.65	0.0042	-1.1	0.088
1749	Q9UGJ9	PGRMC 1	Membrane-associated progesterone receptor component 1/ PGRMC1/ mPR	4.56	21772	7/20	26%	122/56	Microsome	Signal transduction	DFTPAELRR RFDGVQDPR	5.37	0.000065	-1.4	0.079	-1.3	0.031
660	Q9HCC0	MCCC2	Methylcrotonoyl-CoA carboxylase beta chain, mitochondrial	7.57	61808	8/28	16%	62/56	Mitochondrion	Metabolism	ALVNQLHER FLYIWPNAR	1.61	0.016	1.06	0.72	1.03	0.83
1551	Q9UI28	METTL 11A	Methyltransferase-like protein 11A	5.32	25770	6/23	29%	69/56	Cytoplasm	Biosynthesis	RLLLPLFR LLLPLFR	1.35	0.0001	-1.53	0.0047	-1.09	0.015

1006	Q5CZI7	MAPT	Microtubule-associated protein tau	6.25	79108	7/30	9%	57/56	Cytoplasm	Cytoskeletal organization	QPAAAPRGKPVSR TDHGAEIVYK	-1.52	0.00004	-1.14	0.17	-1.05	0.51
1555	O75489	NDUFS3	NADH dehydrogenase [ubiquinone] iron-sulfur protein 3, mitochondrial/NADH-ubiquinone oxidoreductase 30 kDa subunit	6.99	30337	6/23	21%	68/56	Mitochondrion	Electron transport	FEIVYNLLSLR DFPLSGYVELR	-1.25	0.00055	-2.26	0.00068	-1.05	0.26
987	Q9UI06	NSFL1C	NSFL1 cofactor p47/UBX domain-containing protein 2C	4.99	40548	6/24	17%	74/56	Golgi	Vascular transport	FYAGGSER GEVPAELR	1.1	0.035	-1.64	0.036	-1.2	0.031
1450	Q9NSY0	NRBP2	Nuclear receptor-binding protein 2[d]	6.05	58280	1/1	1%	37/29	Cytoplasm	Cell differentiation	MAAPEPAPRR	1.25	0.013	-1.64	0.014	-1.22	0.0077
1192	Q12826	NPM1	Nucleophosmin	4.64	32726	6/19	19%	65/56	Nucleus	Protein folding	VDNDENEHQLSLR MTDQEAIQDLWQWR	1.68	0.00059	-2.01	0.012	-1.26	0.0037
1193	Q12826	NPM1	Nucleophosmin	4.64	32726	8/17	25%	70/56	Nucleus	Protein folding	VDNDENEHQLSLR AKMQASIEK	1.75	0.0003	-1.9	0.015	-1.26	0.0076
1692	P62937	PPIA	Peptidyl-prolyl cis-trans isomerase A/cyclophilin A	7.68	18229	9/22	47%	97/56	Cytoplasm	Protein folding	VSFELFADKVPK IIPGFMCQGGDFTR EGMNIVEAMER	2.43	0.000089	-2.13	0.000096	-1.21	0.035
1691	P62937	PPIA	Peptidyl-prolyl cis-trans isomerase A/cyclophilin A[d]	7.68	18229	9/27 (1/1)	43% (10%)	77/56 (38/29)	Cytoplasm	Protein folding	IIPGFMCQGGDFTR (VNPTVFFDIAVDGEPLGR)	1.82	0.000051	-1.85	0.0036	-1.25	0.0042
1645	P32119	PRDX2	Peroxiredoxin-2	5.66	22049	9/30	32%	96/56	Cytoplasm	Redox regulation	RLSEDYGVLK QITVNDLPVGR	1.62	2.8E-06	-1	0.92	-1.08	0.071
1502	P18669	PGAM1	Phosphoglycerate mutase1	6.67	28900	13/38	55%	135/56	Cytoplasm	Metabolism	**FSGWYDADLSPAGHEEAKR** ALPFWNEEIVPQIK	1.04	0.22	-2.77	0.000069	-1.37	0.00038
1085	Q96AW2	PSAT1	Phosphoserine aminotransferase/PSAT	7.56	40796	9/24	26%	116/56	Cytoplasm	Metabolism	IINNTENLVR FGVIFAGAQK AEDNADTLALV	1.53	0.0007	1.1	0.24	1.02	0.55

Spot No.	swiss-prot No.	Gene name	Protein name	pI	MW	No. Match.	Cov. (%)	Score	Subcellular location	Functional ontology	matched peptides[e]	Dx5 / SA[a]	T-test	SA + Do x 0.1μ M / SA[b]	T-test	Dx5 + Dox 0.1 μ M / Dx5[c]	T-test
1381	P12004	PCNA	Proliferating cell nuclear antigen/PCNA	4.57	29092	7/19	26%	74/56	Nucleus	Gene regulation	FEAPNQEK FSASGELGNGNI K	1.63	0.0011	-1.24	0.029	-1.01	0.92
1721	Q8WU70	PTGES3	Prostaglandin E synthase 3 / Telomerase-binding protein p23 / Hsp90 co-chaperone / cPGES	4.35	18971	5/17	29%	62/56	Cytoplasm	Protein folding	SILCCLR GESGQSWPR	1.26	0.031	-1.55	0.0013	-1.19	0.1
1461	Q9UL46	PSME2	Proteasome activator complex subunit 2/PSME2	5.44	27515	9/19	26%	90/56	Proteasome	Protein degradation	ETHVMDYR DEAAYGELR	1.1	0.00049	1.54	0.000084	1.56	0.00068
1618	P49721	PSMB2	Proteasome subunit beta type-2	6.51	22993	6/20	35%	82/56	Cytoplasm	Protein degradation	YYTPTISR FILNLPTFSVR	1.15	0.087	1.84	0.0018	1.21	0.055
1616	P28070	PSMB4	Proteasome subunit beta type-4	5.72	29242	7/23	22%	72/56	Cytoplasm	Protein degradation	QPVLSQTEAR FEGGVVIAADM LGSYGSLAR	1.68	0.039	-1.12	0.48	-1.11	0.66
767	P30101	PDIA3	Protein disulfide-isomerase A3/ERp57/p58	5.98	57146	15/39	24%	94/56	ER	Protein folding	LAPEYEAAATR FVMQEEFSR	-1.01	0.77	-1.86	0.0046	-1.28	0.0015
744	P07237	P4HB	Protein disulfide-isomerase/PDI	4.76	57480	8/45	18%	76/56	ER	Protein folding	TVIDYNGER YKPESEELTAER	1.28	0.000042	-1.63	0.0053	-1.19	0.0033
1632	Q99497	PARK7	Protein DJ-	6.33	20050	10/19	54%	106/56	Cytoplasm	Redox regulation	MMNGGHYTYS ENR GAEEMETVIPV DVMR	1.02	0.34	-2.08	0.0027	-1.22	0.0037
1465	P00491	PNP	Purine nucleoside phosphorylase	6.45	32325	11/23	36%	129/56	Cytoplasm	Immune response	FEVGDIMLIR FPAMSDAYDR	-1.12	0.0055	1.55	0.00011	1.12	0.091
1526	Q9NVS9	PNPO	Pyridoxine-5'-phosphate oxidase	6.62	30311	6/20	26%	72/56	Cytoplasm	Biosynthesis	FFTNFESR GEEDWLYER	1.25	0.002	-1.64	0.018	-1.11	0.021
1395	Q9UFK3	PDHB	Pyruvate dehydrogenase E1 component subunit beta, mitochondrial/PDHE1-B	6.2	39550	6/10	18%	62/56	Mitochondrion	Metabolism	VTGADVPMPY AK IMEGPAFNFLD APAVR	1.11	0.03	-1.75	0.00076	-1.2	0.051
909	Q9UQM6	GDI2	Rab GDP dissociation inhibitor beta/GDI2	6.11	51087	7/17	18%	71/56	Cytoplasm	Vascular transport	IKLYSESLAR DLGTESQIFISR SITRSYYR	-1.26	0.00093	1.33	0.00032	1.5	0.00085

1147	Q8WUD1	RAB2B	Ras-related protein Rab-2B	7.68	24427	5/23	25%	62/56	Cytoplasm	Vascular transport	QHSSSNMVIMLIGNK	-1.06	0.31	2.03	0.000065	1.53	0.0019
1675	Q92601	RB1CC1	RB1-inducible coiled-coil protein 1	5.3	185085	5/8	4%	58/56	Nucleu	Cell cycle	TTFSTENDMEIKSTMQQQER	1.23	0.0099	-3.35	0.00012	-1.32	0.015
1103	Q15293	RCN1	Reticulocalbin-1	4.86	38866	5/18	19%	60/56	ER	Signal transduction	HWILPQDYDHAQAEAREQFNEFR	1.81	7.1E-06	-1.49	0.0057	-1.29	0.01
786	P00352	ALDH1A1	Retinal dehydrogenase 1 / Aldehyde dehydrogenase family 1 member A1 / RALDH 1	6.3	55454	13/39	24%	99/56	Cytoplasm	Biosynthesis	QAFQIGSPWRYCAGWADKIQGR	-1.93	0.000035	-1.02	0.69	-1.17	0.0094
784	P00352	ALDH1A1	Retinal dehydrogenase 1 / Aldehyde dehydrogenase family 1 member A1 / RALDH 1	6.3	55454	8/15	16%	68/56	Cytoplasm	Biosynthesis	QAFQIGSPWRTIPIDGNFFTYTR	-1.82	0.000047	1.09	0.47	-1.01	0.89
957	P13489	RNH1	Ribonuclease inhibitor / Placental RNase inhibitor	4.71	51766	9/25	32%	96/56	Cytoplasm	Gene regulation	SLDIQSLDIQCEELSDARWAELLPLLQQCQVVR	1.77	0.00054	1.14	0.13	-1.05	0.46
1383	P11908	PRPS2	Ribosphate pyrophosphokinase 2	6.15	35146	7/18	30%	88/56	Cytoplasm	Biosynthesis	VTAVIPCFPYARIQVIDISMILAEAIR	1.58	0.000017	1.1	0.091	-1.06	0.081
673	Q08209	PPP3CA	Serine/threonine-protein phosphatase 2B catalytic subunit alpha isoform / Calmodulin-dependent calcineurin A subunit alpha isoform / CAM-PRP catalytic subunit	5.58	59335	6/14	12%	61/56	Nucleus	Signal transduction	AVPFPPSHRAHEAQDAGYR	-4.23	0.000024	1.2	0.079	-1.02	0.82
1397	Q15511	SR	Spermidine synthase	5.3	34373	8/12	29%	107/56	Cytoplasm	Metabolism	SRYQDILVFRYQDILVFR	1.12	0.038	1.5	0.011	1.02	0.76
634	P31948	STIP1	Stress-induced-phosphoprotein 1/STI1	6.4	63227	13/30	23%	98/56	Cytoplasm	Protein folding	AAALEFLNRYKDAIHFYNK	1.31	0.02	-1.76	0.0028	-1.26	0.055
1214	Q9Y2Z0	SUGT1	Suppressor of G2 allele of SKP1 homolog	5.07	41284	8/19	25%	95/56	Cytoplasm	Cell Cycle	SLELNPNNSTAMLRNLYPSSSPYTR	2.62	0.000014	-2.15	0.0041	-1.32	0.00034

Spot No.	swiss-prot No.	Gene name	Protein name	pI	MW	No. Match.	Cov. (%)	Score	Subcellular location	Functional ontology	matched peptides[e]	Dx5 / SA[a]	T-test	SA + Do x 0.1μ M / SA[b]	T-test	Dx5 + Dox 0.1 μ M / Dx5[c]	T-test
1744	Q8NBS9	TXNDC5	Thioredoxin domain-containing protein 5/ERp46	5.63	48283	7/24	18%	64/56	ER	Redox regulation	GYPTLLWFR KEFPGLAGVK	-1.01	0.82	-1.63	0.019	-1.19	0.001
1303	O43396	TXNL1	Thioredoxin-like protein 1	4.84	32630	4/18	24%	64/56	Cytoplasm	Redox regulation	VGVKPVGSDPD FQPELSGAGSR ISYFTFIGTPVQA TNMNDFK	1.09	0.11	-1.5	0.000036	-1.18	0.017
1731	Q96J01	THOC3	THO complex subunit 3	5.7	39431	7/14	15%	77/56	Nucleus	Transcription regulation	YVLGMQELFR RPLLAFACDDK	1.01	0.76	1.54	0.00042	1.09	0.13
1208	P37837	TALDO1	Transaldolase	6.36	37688	8/16	18%	67/56	Cytoplasm	Metabolism	IYNYYKK TIVMGASFR	-1.42	0.0051	1.7	0.000015	1.46	0.0053
1181	Q8WV32	TALDO1	Transaldolase	6.36	37688	11/30	27%	96/56	Cytoplasm	Metabolism	LSFDKDAMVAR SYEPLEDPGVK	-1.18	0.0049	2.1	0.00037	1.73	0.0014
1720	Q9UC70	TPT1	Translationally-controlled tumor protein / TCTP/Fortilin	4.84	19697	9/27	45%	98/56	Cytoplasm	Cytoskeleton	YIKDYMK HILANFK	-1.09	0.033	-1.73	0.0044	-1.16	8.8E-06
1548	P60174	TPI1	Triosephosphate isomerase/TPI	5.65	31057	16/35	68%	196/56	Cytoplasm	Metabolism	KFFVGGNWK SNVSDAVAQST	1.15	0.13	-2.25	0.0018	-1.11	0.21
1554	Q96AG5	TPI1	Triosephosphate isomerase/TPI	6.45	26938	7/30	33%	78/56	Cytoplasm	Metabolism	IAVAAQNCYK SNVSDAVAQST	1.76	0.0009	-1.78	0.008	-1.14	0.17
766	P23381	WARS	Tryptophanyl-tRNA synthetase, cytoplasmic/IFP53	5.83	53474	7/19	14%	74/56	Cytoplasm	Translational regulation	KPFYLYTGR GIDYDKLIVR	-1.35	0.00026	1.65	6.7E-06	-1.02	0.49
1567	P09936	UCHL1	Ubiquitin carboxyl-terminal hydrolase isozyme L1 / Ubiquitin thioesterase L1	5.33	25151	8/30	39%	81/56	Cytoplasm	Protein degradation	EFTEREQGEVR NEAIQAAHDAV AQEGQCR	-1.11	0.08	-1.67	0.014	-1.15	0.052
1561	Q8N1D5	C1orf158	Uncharacterized protein C1orf158	9.73	23110	5/15	23%	64/56	Unknown	Unknown	VLTGNWMEER TPQSIYR	1	0.98	1.6	0.00027	1.18	0.0054
770	P54727	RAD23B	UV excision repair protein RAD23 homolog B / XP-C repair-complementing complex 58 kDa protein	4.79	43202	7/20	13%	67/56	Nucleus	DNA repair	AVEYLLMGIPG DR NQPQFQQMR	-1.14	0.02	-1.79	0.0013	-1.27	0.00092
440	Q15942	ZYX	Zyxin	6.22	62436	6/17	10%	61/56	Cytoplasm	Cytoskeleton	FGPVVAPKPK QNVAVNELCGR	1.64	0.0023	1.1	0.65	-1.13	0.16

(Bruker Daltonics) in reflector mode and the raw data was analyzed with FlexAnalysis acquisition software (version 3.0, Bruker Daltonics). The algorithm used for spectral annotation was SNAP (Sophisticated Numerical Annotation Procedure). The following metrics were used: peak detection algorithm: SNAP; signal to noise threshold: 25; relative intensity threshold: 0%; minimum intensity threshold: 0; maximal number of peaks: 50; quality factor threshold: 1000; SNAP average composition: averaging; baseline subtraction: median; flatness: 0.8; and median level: 0.5. The spectrometer was also calibrated with a peptide calibration standard (Bruker Daltonics) and internal calibration was performed using trypsin autolysis peaks at *m/z* 842.51 and *m/z* 2211.10 (MS BioTools version 3.0, Bruker Daltonics). Peaks in the mass range of *m/z* 800–3000 were used to generate a peptide mass fingerprint that was searched against the Swiss-Prot/TrEMBL database (20080918) with 397539 entries using Mascot software v2.2.06 (Matrix Science, London, UK). The following parameters were used for the search: *Homo sapiens*; tryptic digest with a maximum of 1 missed cleavage; carbamidomethylation of cysteine, partial protein N-terminal acetylation, partial methionine oxidation and partial modification of glutamine to pyroglutamate and a mass tolerance of 50 ppm. Identification was accepted based on significant MASCOT Mowse scores ($p<0.05$), spectrum annotation and observed versus expected molecular weight and pI on 2-DE. MALDI-TOF/TOF analysis was performed in LIFT mode using the same instrument. MS/MS ion searches were performed using Mascot with the same search parameters as above and using an MS/MS tolerance of ±0.2 Da.

2.9. *Immunoblotting*

Immunoblotting was used to validate the differential expression of mass spectrometry identified proteins. Cells were lysed with a

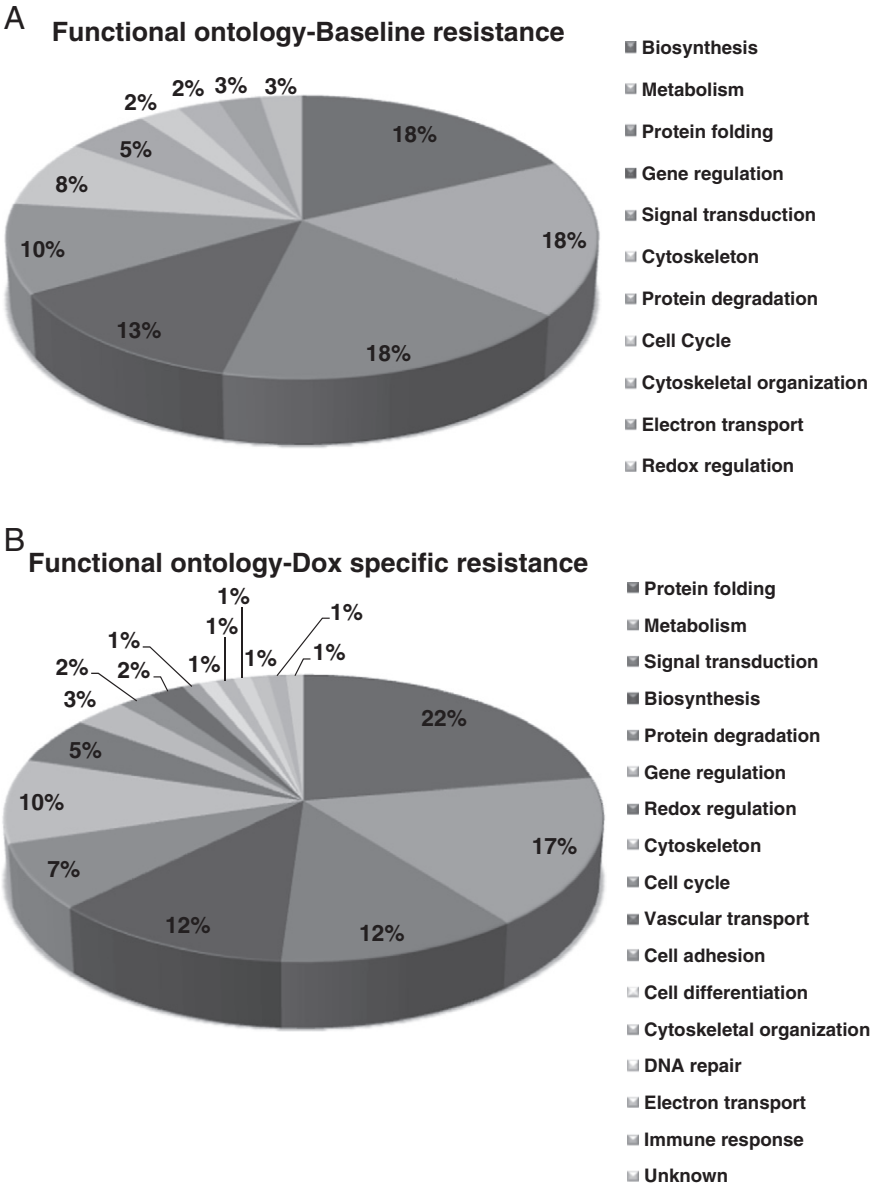

Fig. 3 – Functional classification of identified proteins correlated to (A) baseline resistance and (B) doxorubicin specific resistance in uterine cancer by 2D-DIGE/MALDI-TOF MS.

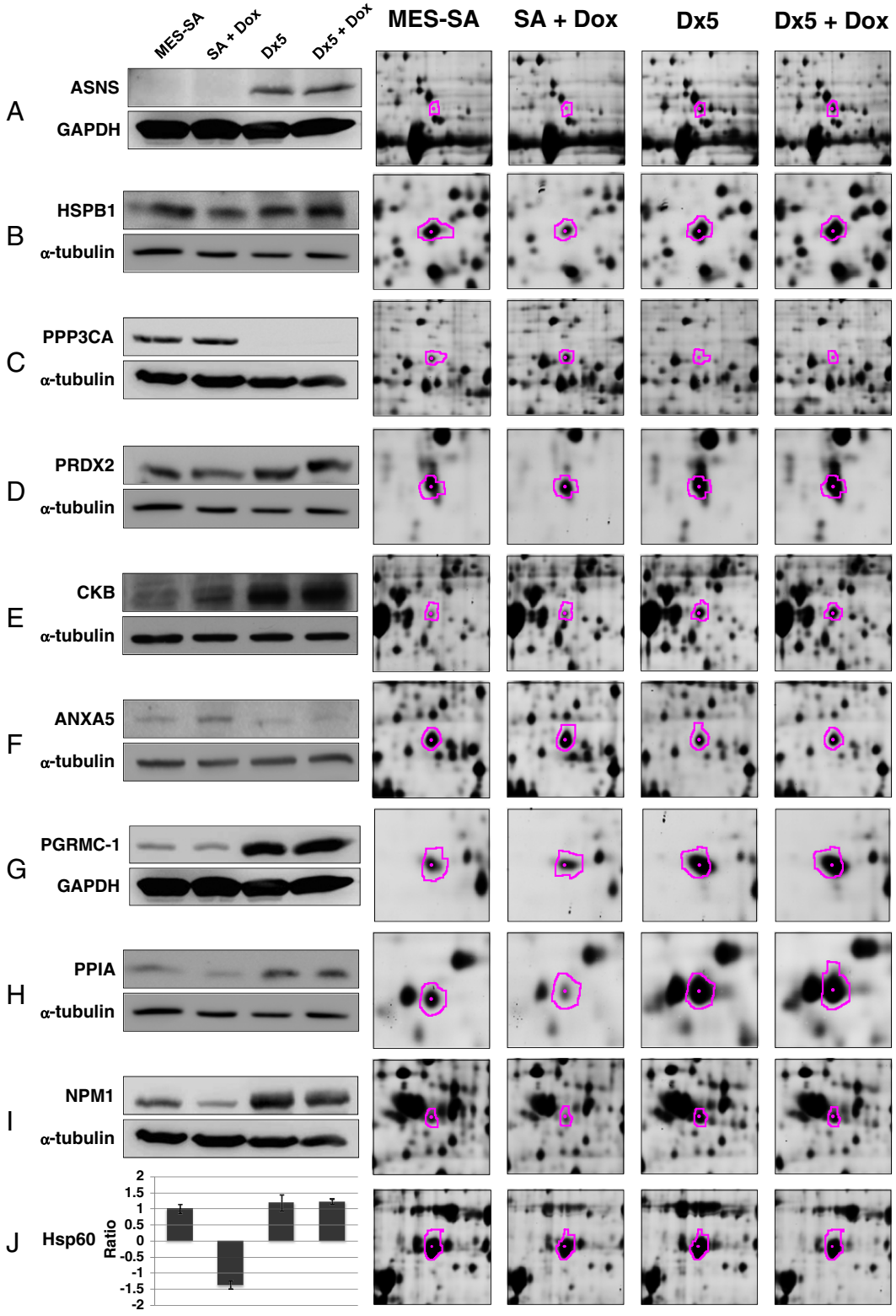

Fig. 4 – Representative immunoblotting and ELISA analyses for selected differentially expressed proteins identified by proteomic analysis in MES-SA and MES-SA/Dx5 treated with/without doxorubicin. The levels of identified proteins including (A) ASNS, (B) HSP-27, (C) calcineurin A, (D) peroxiredoxin-2, (E) creatine kinase B, (F) annexin A5, (G) mPR, (H) cyclophilin A, (I) nucleophosmin were validated by immunoblotting; while (J) HSP-60 was validated by ELISA in MES-SA and MES-SA/Dx5 treated with/without doxorubicin. The representative immunoblots/ELISA analysis (left panels) and 2D-images of the identified proteins (right panels) were shown in this figure.

lysis buffer containing 50 mM HEPES pH 7.4, 150 mM NaCl, 1% NP40, 1 mM EDTA, 2 mM sodium orthovanadate, 100 μg/mL AEBSF, 17 μg/mL aprotinin, 1 μg/mL leupeptin, 1 μg/mL pepstatin, 5 μM fenvalerate, 5 μM BpVphen and 1 μM okadaic acid prior to protein quantification with Coomassie Protein Assay Reagent (BioRad). 30 μg of protein samples were diluted in Laemmli sample buffer (final concentrations: 50 mM Tris pH 6.8, 10% (v/v) glycerol, 2% SDS (w/v), 0.01% (w/v) bromophenol blue) and separated by 1D-SDS-PAGE following standard procedures. After transferring separated proteins onto 0.45 μm immobilon P membranes (Millipore), the membranes were blocked with 5% w/v skim milk in TBST (50 mM Tris pH 8.0, 150 mM NaCl and 0.1% tween-20 (v/v)) for 1 h. Membranes were incubated in primary antibody solution in TBS-T containing 0.02% (w/v) sodium azide for 2 h. Membranes were washed in TBS-T (3×10 min) and then probed with the appropriate horseradish peroxidase-coupled secondary antibody (GE Healthcare). After washing in TBS-T for 6 times (15 min each), immunoprobed proteins were visualized using an enhanced chemiluminescence method (Visual Protein Co.).

2.10. *Enzyme-linked immunosorbent assay (ELISA)*

EIA polystyrene microtiter plates were coated with 50 μg of protein lysate sample and incubated at 37 °C for 2 h. The plate was washed three times with phosphate buffered saline with tween-20 (PBS-T) and three times with PBS. Plates were then blocked with 100 μL of 5% skim milk in PBS at 37 °C for 2 h and then washed three times with PBST. Antibody (Abcam) solution was added and incubated at 37 °C for 2 h. After washing with PBST and PBS for 10 times in total, 100 μL of peroxidise-conjugated secondary antibody in PBS was added for incubation at 37 °C for 2 h. Following 10 washes, 100 μL of 3,3′,5,5′-tetramethyl benzidine (Pierce) was added. After incubation at room temperature for 30 min, 100 μL of 1 M H_2SO_4 was added to stop the reaction and the absorbance at 450 nm measured using a Stat Fax 2100 microtiter plate reader (Awareness Technology Inc. FL, USA).

2.11. *siRNA design, construction and transfection*

The siRNA against mPR and ASNS was synthesized by Invitrogen. The targeting sequences 5′-AAU UUG CGG CCU UUG GUC ACA UCG A-3′ and 5′-AGU GAA CUG AGA CUC CCA GUC ACU C-3′ against mPR and sequences 5′-UAU CAG AUU GGA AUC CUC AAA CGU C-3′ and 5′-UUG UUU GCU CAA UUC CUC CUU UGU C-3′ against asparagine synthetase were designed and verified to be specific by Blast search against the human genome, and sequences of similar GC contents which do not match any known human coding sequence were used for negative control against mPR and asparagine synthetase. Transfection was mediated with Lipofectamine RNAiMAX (Invitrogen) according to the manufacturer's instruction. Briefly, cells were transfected with 60 nM of mPR siRNA, 100 nM asparagine synthetase siRNA or the corresponding control (pGCsi-control) in serum free medium containing Lipofectamine RNAiMAX for 4 h followed by recovery in medium containing 10% FCS for 24 h. The efficiency of siRNA knockdown was monitored with immunoblotting by using primary antibodies against mPR and asparagine synthetase.

2.12. *Flow cytometry analysis for apoptosis detection*

Annexin-V/propidium iodide (PI) double assay was performed using the Annexin V, Alexa Fluor® 488 Conjugate Detection kit (Life technologies). Following doxorubicin treatment, cells were trypsinized from culture dish and washed twice with cold PBS. 1×10^6 cells were resuspended in 500 μL binding buffer and stained with 5 μL Alexa Fluor 488 conjugated

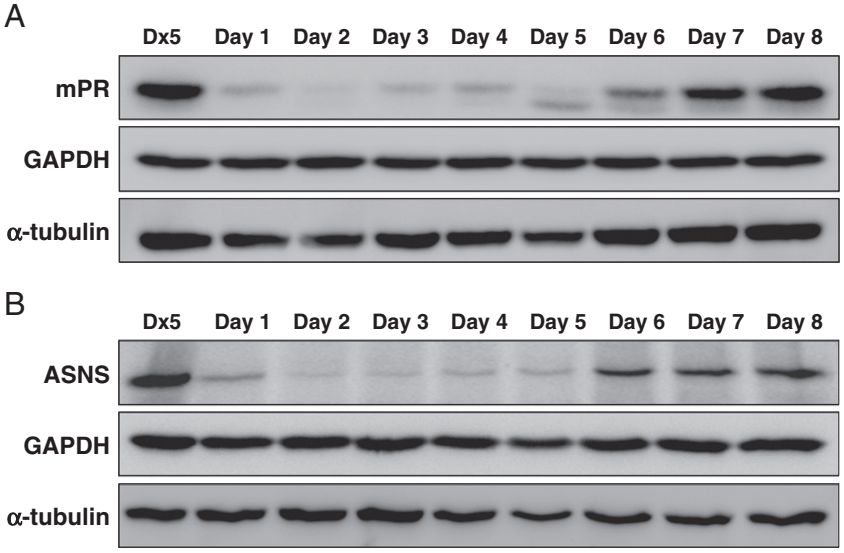

Fig. 5 – Efficiency of mPR siRNA and ASNS siRNA on the inhibition of mPR and ASNS expression in MES-SA/Dx5 cells. MES-SA/Dx5 cells grown overnight were treated with 60 nM mPR-specific siRNA (A) or 100 nM ASAN-specific siRNA (B) for indicated periods. Expression of mPR and ASAN in MES-SA/Dx5 cells were monitored with immunoblotting by using primary antibodies against mPR and ASAN, respectively.

annexin V according to the manufacturer's instructions. 1 μL 100 μg/mL propidium iodide (PI) was added and mixed gently to incubate with cells for 15 min at room temperature in the dark. After incubation period, samples were subjected to FCM analysis in 1 h. using BD Accuri C6 Flow Cytometry (BD Biosciences, San Jose, CA). The data were analyzed using Accuri CFlow® and CFlow Plus analysis software (BD Biosciences).

3. Results

3.1. *Identification of proteins involved in baseline and doxorubicin specific resistance in human uterine cancer cells*

For this study, we prepared a doxorubicin-sensitive uterine cancer cell line, MES-SA, by growing in a doxorubicin-free

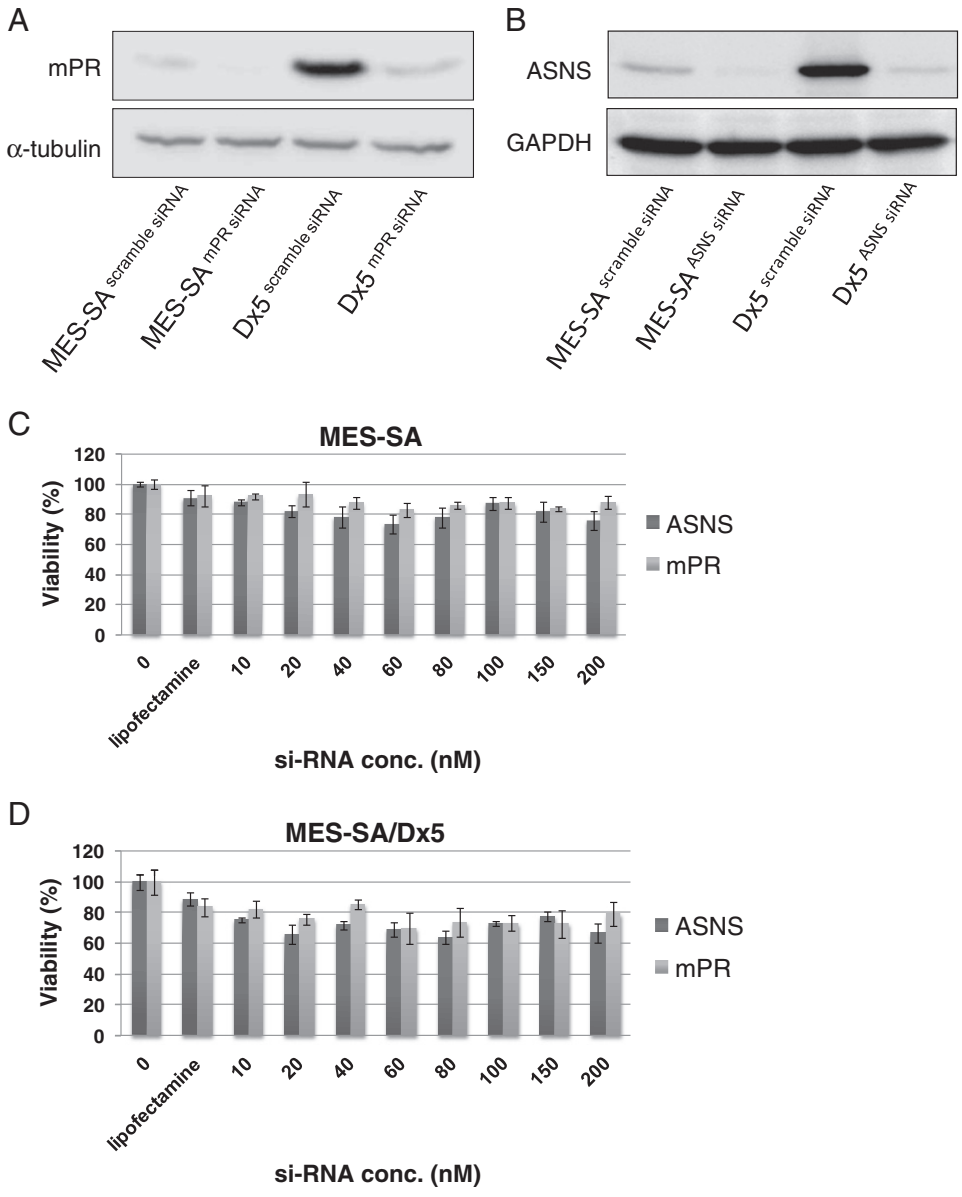

Fig. 6 – Effect of mPR siRNA and ASNS siRNA inhibition on MES-SA and MES-SA/Dx5 cell viability. (A) MES-SA and MES-SA/Dx5 cells grown overnight were pre-treated with 60 nM mPR-specific siRNA or scramble siRNA with similar GC content. Expression of mPR in MES-SA and MES-SA/Dx5 cells was monitored by immunoblotting by using primary antibodies against mPR. (B) MES-SA and MES-SA/Dx5 cells grown overnight were pre-treated with 100 nM ASNS-specific siRNA or scramble siRNA with similar GC content. Expression of ASNS in MES-SA and MES-SA/Dx5 cells was monitored with immunoblotting by using primary antibodies against ASNS. MTT-based viability assays were performed where 500 (C) MES-SA and (D) MES-SA/Dx5 cells seeded overnight were pre-treated with indicated concentrations of mPR-specific siRNA or ASNS-specific siRNA combining with corresponding scramble siRNA. After 24 h, cells were treated with MTT and then DMSO added and the plates shaken for 20 min followed by measurement of the absorbance at 540 nm. Values were normalized against the untreated samples and are the average of 4 independent measurements ±SD.

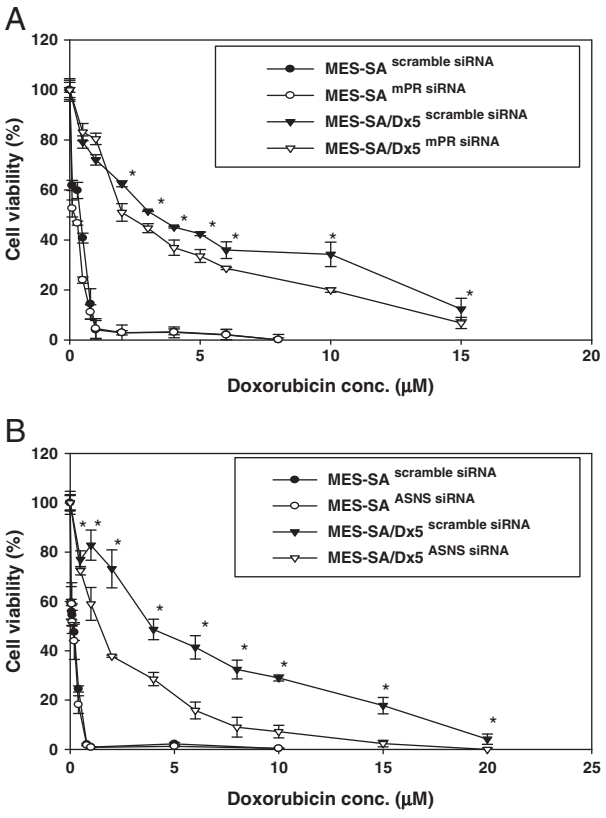

Fig. 7 – Effect of doxorubicin on cell viability of mPR siRNA and ASNS siRNA-silenced MES-SA and MES-SA/Dx5 cells. MTT-based viability assays were performed where 5000 MES-SA and MES-SA/Dx5 cells seeded into 96-well plate for overnight incubation followed by pre-treated with (A) 60 nM mPR-specific siRNA or (B) 100 nM ASNS-specific siRNA combining with corresponding scramble siRNA. After 24 h, cells treated indicated concentrations of doxorubicin for 48 h followed by incubation with MTT and then DMSO added and the plates were shaken for 20 min followed by measurement of the absorbance at 540 nm. Values were normalized against the untreated samples and are the average of 4 independent measurements ± SD.

medium containing 10% (v/v) fetal bovine serum. The MES-SA-resistant cell line, MES-SA/Dx5, was grown under continuous exposure to 0.4 μM doxorubicin to maintain the multiple drug resistance phenotype, and the cells were cultured in a drug-free medium for at least 2 weeks prior to use. The IC_{50} of MES-SA and MES-SA/Dx5 cells were 0.1 μM and 4.3 μM, respectively (Fig. 1A). MES-SA/Dx5 cells showed a significant upregulation in P-glycoprotein and topoisomerase 2 levels (Fig. 1B), demonstrating a difference in doxorubicin resistance between the 2 groups of cells. These distinctly different physiological characteristics made these cell lines appropriate for use as a doxorubicin-resistant cell model for a drug-resistance-associated study.

We used 2D-DIGE to monitor differentially expressed proteins that were associated with baseline resistance and doxorubicin-specific resistance in uterine cancer (Fig. 2A). For baseline resistance analysis, cell lysates from 3 independent MES-SA and MES-SA/Dx5 cultures were analyzed by 2D-DIGE. Triplicates of these 2 different doxorubicin-resistant cell lines were compared simultaneously by 2D-DIGE using pH 3–10 non-linear strips to test a wide range of cellular proteins and provide a global overview of the uterine cancer proteome. The proteomic results indicated that 1755 protein spots could be consistently monitored using this approach (Fig. 2B). In general, the proteomic patterns between MES-SA and MES-SA/Dx5 were similar and only 6.5 % (114 protein spots) displayed greater than a 1.5-fold change in intensity ($p<0.05$) (Fig. 2A and B upper panel), in which 37 protein spots were identified by MALDI-TOF MS as representing 33 different proteins (Table 1 and Supplementary Figs. 1 and 2). Functional classification of these proteins revealed that most were involved in biosynthesis, metabolism, and protein folding (Fig. 3A). To our knowledge, there are no reports of the identification of numerous proteins, including ASNS and mPR, in any doxorubicin-related baseline resistance study. Consequently, these proteins are potential candidates for resistance-related therapy. As expected, 2D-DIGE analysis also identified a number of proteins associated with doxorubicin resistance, including apoptosis regulator Bcl-W and cyclophilin A (Supplementary Table 1).

For doxorubicin-specific resistance analysis, doxorubicin was used at its IC_{50} concentration against MES-SA cells (0.102 μM) to treat both MES-SA and MES-SA/Dx5 cells. As expected, a larger fraction (76% of total identified proteins) of MES-SA-expressed proteins exhibited altered expression levels, compared to only 4.3% of MES-SA/Dx5-expressed proteins (Fig. 2A and B, middle and bottom panels), implying that proteins undergoing significant alterations in doxorubicin-treated MES-SA, but not in MES-SA/Dx5, are crucial to the formation of doxorubicin-specific drug resistance. MALDI-TOF MS produced 87 protein spots, representing 78 different proteins (Table 1 and Supplementary Figs. 1 and 2). Functional classification of these proteins revealed that most were involved in protein folding, metabolism, signal transduction, and biosynthesis (Fig. 3B). There are no literature reports of the identification of numerous proteins, including COP9 signalosome complex subunit 4 in any doxorubicin-related studies. These proteins play important roles in the formation of doxorubicin resistance and, as expected, 2D-DIGE analysis identified a number of proteins known to be associated with doxorubicin-specific resistance, including annexin A5 and TNFR-associated protein 1.

3.2. *Validation of characterized baseline resistance and doxorubicin specific resistance associated proteins via immunoblotting and ELISA analysis*

This proteomic study identified some well-characterized baseline resistance and doxorubicin-specific resistance-associated proteins, such as cyclophilin A and annexin A5. It was essential to validate the expression of these proteins using independent experiments. To this end, we used immunoblot and ELISA analyses to confirm the expression levels of ASNS, calcineurin A, creatine kinase B, mPR, nucleophosmin, HSP-27, peroxiredoxin-2, annexin A5, cyclophilin A, and HSP-60 obtained from MES-SA and MES-SA/Dx5 cell lysates, treated with or without doxorubicin (Fig. 4). We found that ASNS, creatine kinase B, mPR, nucleophosmin, peroxiredoxin-2, and cyclophilin A were

upregulated in MES-SA/Dx5, compared to the levels present in MES-SA. However, calcineurin A antibody showed down-regulation in MES-SA/Dx5 compared to its levels in MES-SA cells. These results confirmed the differential baseline resistance between MES-SA and MES-SA/Dx5. Additionally, a comparison of protein levels between MES-SA and MES-SA/Dx5 cells treated or untreated with 0.1 μM doxorubicin (doxorubicin's IC_{50} concentration against MES-SA) revealed that nucleophosmin, HSP-27, annexin A5, and cyclophilin A exhibit significant alterations in doxorubicin-treated MES-SA, but not in MES-SA/Dx5 cells. This observation confirmed that these differentially expressed proteins are associated with doxorubicin-specific resistance in uterine cancer. Overall, our immunoblotting results and ELISA analyses are in agreement with the 2D-DIGE analysis results.

3.3. *Evaluation of the roles of mPR and ASNS on doxorubicin resistance in uterine cancer using siRNA knockdown*

We found that ASNS and mPR are overexpressed in doxorubicin-resistant MES-SA/Dx5 cells compared to doxorubicin-sensitive MES-SA cells; these 2 proteins are among the most differentially expressed proteins identified by our proteomic analysis. We performed knockdown experiments in MES-SA and MES-SA/Dx5 cells to evaluate the roles of mPR and ASNS in doxorubicin resistance. Immunoblot analysis showed greater than 90% efficiency in the reduction of endogenous mPR and ASNS protein levels when alpha-tubulin and GAPDH were the internal standards. We could maintain ASNS and mPR knockdown efficiency for more than 5 days (Figs. 5, and 6A, B). Knockdown of mPR and ASNS with the indicated concentrations of siRNA results in significantly reduced viability in the MES-SA and MES-SA/Dx5 cells, with reductions in viability of approximately 20% and 30%, respectively (Fig. 6C and D). MTT assay revealed no decreased viability in mPR knockdown MES-SA cells, and a 35% reduction in the viability of mPR knockdown MES-SA/Dx5 cells following treatment with the indicated concentrations of doxorubicin compared to scramble siRNA transfected controls (Fig. 7A). Additionally, viability assay of ASNS knockdown MES-SA cells showed no reduction in cell viability, whereas ASNS knockdown MES-SA/Dx5 cell viability (transfected with scramble siRNA) was decreased by 70% compared to controls following treatment with the indicated concentrations of doxorubicin (Fig. 7B).

We used flow cytometry with propidium iodide staining and annexin V-conjugated Alexa Fluor 488 to analyze the percentages of apoptotic MES-SA cells and MES-SA/Dx5 cells induced by various concentrations of doxorubicin treatment, with or without mPR or ASNS knockdown. The total number of apoptotic cells is represented by the numbers of early apoptotic cells plotted in the LR quadrant and late apoptotic cells displayed in the UR quadrant of the resulting histograms. We found that treatment of doxorubicin at the doses from $0\times IC_{50}$ to $2\times IC_{50}$ increases the percentages of total apoptotic cells (LR+UR) in MES-SA from 15.1% to 37.3% compared with changes from 14% to 39.2% in mPR knockdown MES-SA cells. Thus, mPR has no direct effect on doxorubicin-induced MES-SA cell apoptosis (Fig. 8A). By contrast, doxorubicin treatment of MES-SA/Dx5 cells from $0\times IC_{50}$ to $2\times IC_{50}$ increases the percentages of total apoptotic cells (LR+UR) from 17.9% to 56.6% compared with changes from 21.3% to 59.4% in mPR knockdown MES-SA/Dx5 cells, whereas the number of late apoptotic cells (UR) in MES-SA/Dx5 and mPR knockdown MES-SA/Dx5 cells showed increases from 8.7% to 47% and from 10.5% to 52.8%, respectively. These results indicated that mPR has a minor effect on doxorubicin-induced late apoptosis in MES-SA/Dx5 cells, but has no significant effect on the total number of doxorubicin-induced apoptotic MES-SA/Dx5 cells (UR+LR) (Fig. 8B).

Further study on ASNS showed that treatment of MES-SA cells with doxorubicin at doses from $0\times IC_{50}$, to $2\times IC_{50}$ increased the number of total apoptotic cells (LR+UR) from 19.2% to 58.2%, compared with increases ranging from 22.5% to 59.8% in ASNS knockdown MES-SA cells. These results indicated that ASNS has no direct effect on doxorubicin-induced MES-SA cell apoptosis (Fig. 8C). By contrast, we found that treatment of MES-SA/Dx5 cells with doxorubicin at doses from $0\times IC_{50}$ to $2\times IC_{50}$ increased the number of apoptotic cells (LR+UR) from 14.4% to 64%, compared with increases from 30.8% to 83.6% in ASNS knockdown MES-SA/Dx5 cells, whereas the percentages of late apoptotic cells (UR) were increased from 7.9% to 53.8%, and from 15.7% to 76.1% in MES-SA/Dx5 and ASNS knockdown MES-SA/Dx5 cells, respectively. This finding indicates that ASNS plays a significant role in mediating doxorubicin-induced apoptosis in MES-SA/Dx5 cells, and that this mediation occurs predominantly during late-stage apoptosis (Fig. 8D).

The number of total apoptotic cells (LR+UR) in mPR or ASNS knockdown MES-SA and that in MES-SA/Dx5 cells are greater than the number for parental MES-SA or MES-SA/Dx5 cells, implying that mPR RNAi or ASNS RNAi alone is sufficient to induce MES-SA and MES-SA/Dx5 cellular apoptosis. This effect is considerably more significant in doxorubicin resistant MES-SA/Dx5 cells than it is in doxorubicin sensitive MES-SA cells.

4. Discussion

A better understanding of chemotherapy-related drug resistance mechanisms is needed to provide opportunities for the diagnosis and therapy of cancer. Most of the functional information on cancer chemoresistance was acquired from transcription-level studies, rather than from translation-level studies. Past research into drug resistance mechanisms started with a known single-marker candidate. We adopted an innovative global, high-resolution, and high-throughput proteomic approach based on 2D-DIGE coupled with MALDI-TOF/TOF MS to identify proteins that were differentially expressed in the doxorubicin-resistant human uterine cancer cell line, MES-SA/Dx5, and its parental cell line MES-SA, to provide a complete view of protein expression and protein–protein interactions. We observed 114 MALDI-identified protein spots that showed significant differences either in expression between the 2 cell lines, or in protein expression resulting from doxorubicin-induced changes. Ten proteins were identified by immunoblotting and ELISA analysis using commercially available antibodies. We validated the functions of mPR and ASNS in drug resistance, and found that their overexpressions contribute significantly to the

development of doxorubicin resistance in MES-SA/Dx5 cells. Our findings demonstrate that multiple processes are involved in the development of drug resistance in uterine cancer cells, and that these different mechanisms may contribute to chemotherapeutic resistance in the treatment of uterine cancer.

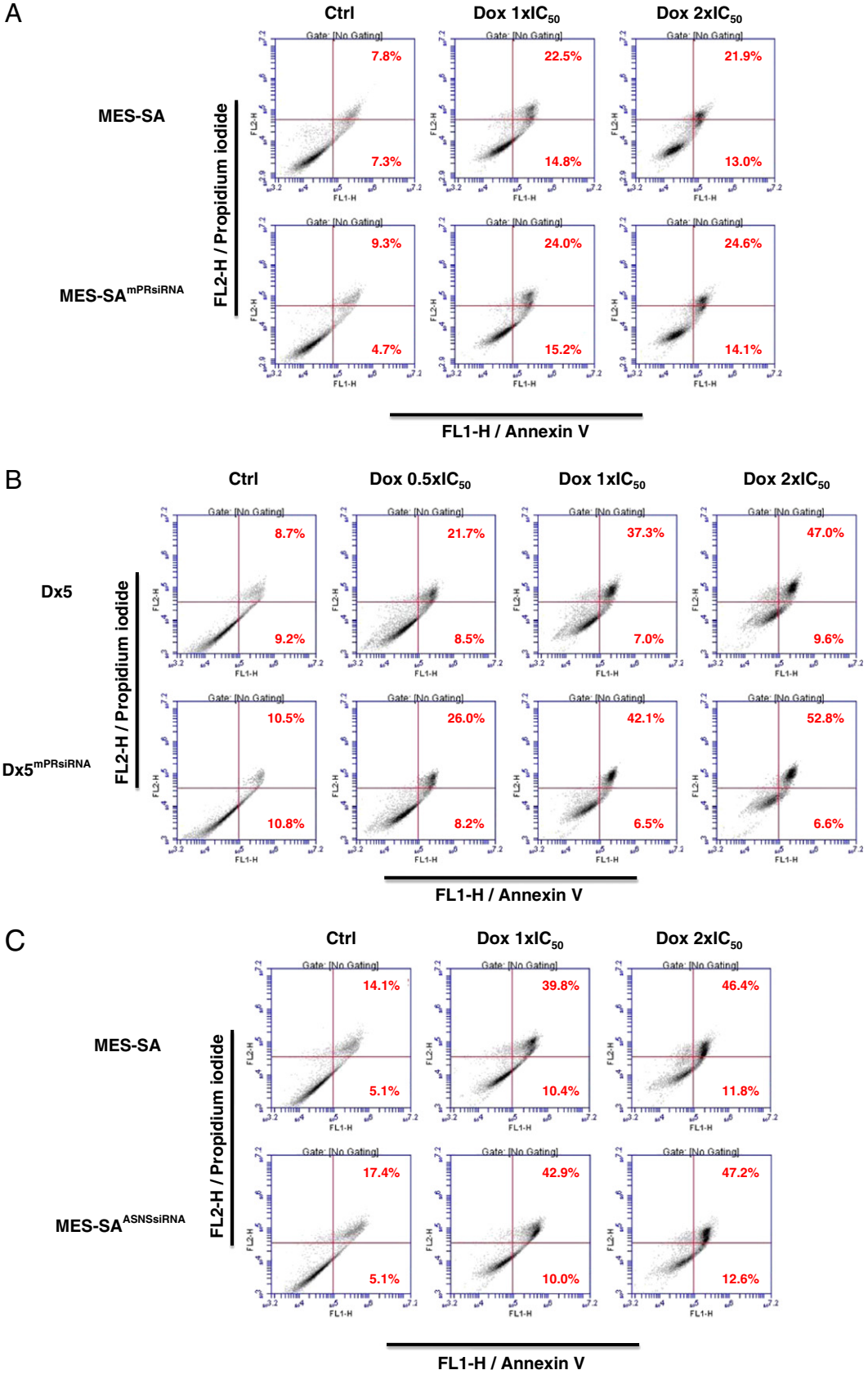

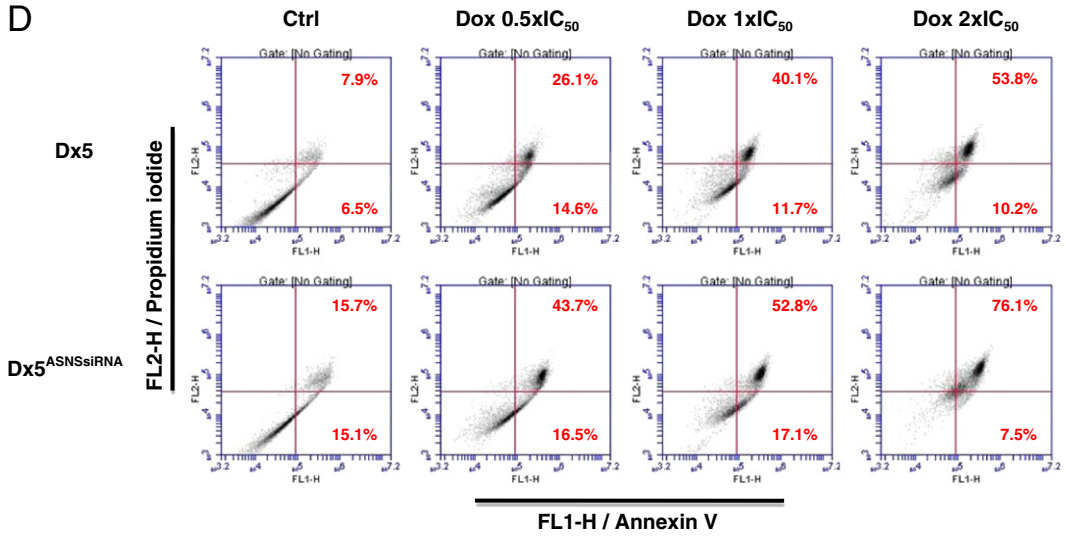

Fig. 8 – Treatment of doxorubicin with a dose-dependent manner induced apoptosis in mPR siRNA and ASNS siRNA-silenced MES-SA and MES-SA/Dx5 cells. MES-SA and MES-SA/Dx5 cells were treated with indicated concentrations of doxorubicin or left untreated for 48 h. After treatment, 10^6 cells were incubated with Alexa Fluor 488 and propidium iodide in 1× binding buffer at room temperature for 15 min, and then stained cells were analyzed by flow cytometry to examine: (A) effect of doxorubicin on apoptosis in MES-SA and mPR siRNA silenced MES-SA cells. (B) Effect of doxorubicin on apoptosis in MES-SA/Dx5 and mPR siRNA silenced MES-SA/Dx5 cells. (C) Effect of doxorubicin on apoptosis in MES-SA and ASNS siRNA silenced MES-SA cells. (D) Effect of doxorubicin on apoptosis in MES-SA/Dx5 and ASNS siRNA silenced MES-SA/Dx5 cells. Annexin V is presented in x-axis as FL1-H, and propidium iodide is presented in y-axis as FL2-H. LR quadrant indicates the percentage of early apoptotic cells (annexin V positive cells), and UR quadrant indicates the percentage of late apoptotic cells (annexin V positive and propidium iodide positive cells).

We determined numerous potential biological functions of the identified proteins toward baseline resistance and doxorubicin-specific resistance in human uterine cancer cells using a Swiss-Prot search combined with KEGG pathway analysis. Our findings should be useful for a systematic study on the mechanisms of doxorubicin resistance in uterine cancer. Fig. 9 shows a comparison of the expression profiles of the differentially expressed proteins for both baseline and doxorubicin-specific resistance. Proteins known to regulate biosynthesis, redox regulation, gene regulation, and protein folding are upregulated in MES-SA/Dx5, but not in MES-SA, implying that doxorubicin-resistant cells have greater ability to maintain cellular protein conformation, redox modification of cellular proteins, gene expression, and biomacromolecule formation. For example, the induced expression of redox-regulated proteins such as peroxiredoxins in resistant cells may account for cancer progression and invasiveness [16].

Doxorubicin drug resistance mechanisms adopted by uterine cancer cells involve drug efflux and anti-apoptosis responses. Doxorubicin diffuses into intracellular spaces to increase its cellular concentrations. P-glycoprotein (P-gp), an energy-demanding efflux transporter in the plasma membrane, is able to pump doxorubicin out of cells using ATP from phosphocreatine as an energy source. P-glycoprotein overexpresses in MES-SA/Dx5 cells; thus, we propose that the overexpression of creatine kinase in MES-SA/Dx5 increases the capacity of phosphocreatine catabolism to generate ATP for P-gp activity during drug efflux. Doxorubicin treatment increases expression of ANXA7, which blocks the phosphorylation of RB protein, resulting in G1 phase arrest [17]. By contrast, the insignificant changes in ANXA7 levels in doxorubicin-treated MES-SA/Dx5 cells indicate that ANXA7 might play a critical role in inducing resistant cells escaping G1 phase arrest; MBP-1, the translated form of ENO-1, negatively regulates c-Myc gene expression, and thus, inhibits cell apoptosis [18]. This implies that resistant cells avoid doxorubicin-induced cell death by preventing the downregulation of ENO-1. A recent report indicated that cyclophilin A (Cyp A) acts as a negative regulator of apoptosis by sequestering cytochrome c [19]. Thus, the overexpression of Cyp A offers a strategy for resistant cells to escape doxorubicin-induced cell death through the inhibition of cytochrome C release. Additionally, a recent study reported that overexpression of ERp29 attenuates doxorubicin-induced cell apoptosis through the upregulation of Hsp27 in breast cancer cells, and that upregulation of ERp29 and Hsp27 was detected in doxorubicin-resistant breast cancer cells [20]. This observation is in partial agreement with our current study, in which we found that neither ERp29 nor Hsp27 exhibits significant changes in expression following doxorubicin treatment of MES-SA/Dx5 cells, but are downregulated in MES-SA cells. Moreover, ERp29 may downregulate eIF2α expression, and further stimulate Hsp27 activity. This process might alleviate misfolded and unfolded protein-induced ER stress in resistant cells. During catabolism, the mitochondrial electron transport system degrades intracellular doxorubicin to its semiquinone form. The semiquinone subsequently reacts with iron, hydrogen

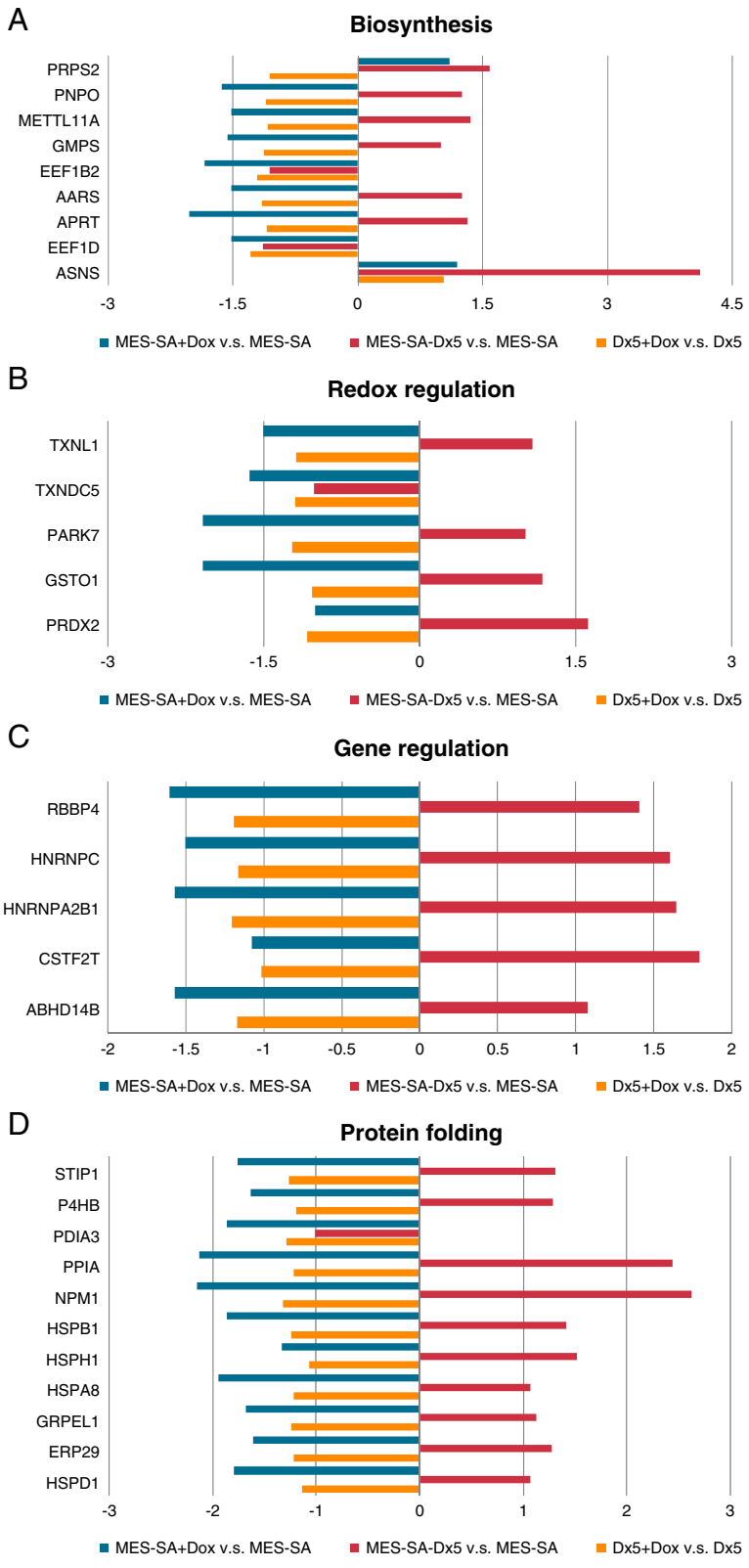

Fig. 9 – Expression profiles for differentially expressed proteins potentially contributing to: (A) biosynthesis and (B) redox regulation, (C) gene regulation and (D) protein folding in MES-SA and MES-SA/Dx5 treated with/without doxorubicin. The horizontal bars represent fold-changes in protein expression and the vertical axis indicates the identified proteins. Additional details for each protein can be found in Table 1.

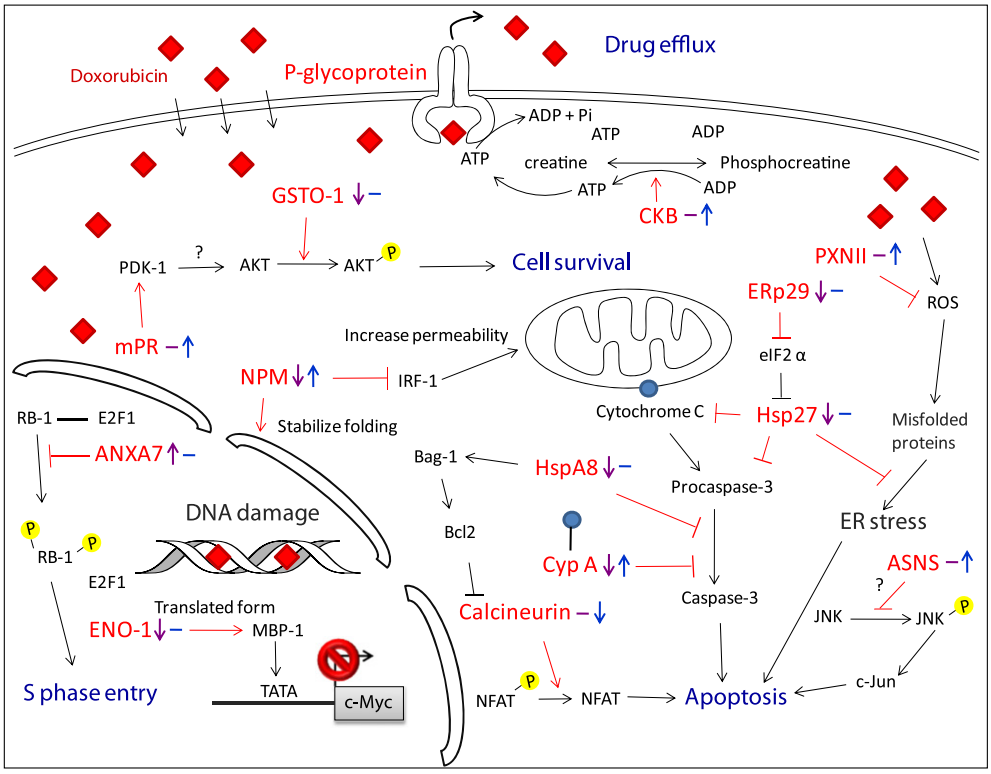

Fig. 10 – A hypothetical model of doxorubicin drug-resistance in uterine cancer. The proposed doxorubicin-resistance mechanisms used by uterine cancer cells involve drug efflux and anti-apoptosis processes. Doxorubicin diffuses into intracellular spaces to increase its concentration within cells. P-glycoprotein is able to pump doxorubicin out of cells that rely on phosphocreatine through creatine kinase as an energy source. Treatment with doxorubicin results in upregulated ANXA7 expression, and ANXA7 then blocks phosphorylation of the RB protein, allowing resistant cells to escape G1 arrest. MBP-1 negatively regulates c-Myc gene expression, promoting cell survival, implying that resistant cells prevent doxorubicin-induced cell death through decreased expression of ENO-1. Drug resistant cells sequester calcineurin and inhibit Fas/FasL dependent apoptosis through de-phosphorylation of NEAT by calcineurin [31]. Additionally, NPM1 protects resistant uterine cancer cells from doxorubicin exposure, and shows upregulation in drug-resistant cells. Overexpression of NPM1 in resistant cells might also inhibit IRF-1 activity, decreasing mitochondrial permeability and inhibiting doxorubicin-induced programed cell death. Cyp A is an anti-apoptosis factor, which inhibits pro-caspase3 activation by binding to cytochrome C. The observed overexpression of Cyp A implies that resistant cells escape doxorubicin-induced cell death by inhibiting caspase3 activation. ERp29 downregulates eIF2α expression and further stimulates Hsp27 activity; this process alleviates ER stress in resistant cells induced by misfolded and unfolded proteins. The observation that there is no significant change in Hsp27 expression in resistant cells during doxorubicin exposure indicates the blockage of apoptosis by sequestration of cytochrome C. Doxorubicin-induced ROS is scavenged by PXN2, preventing the accumulation of misfolded proteins in drug-resistant cells. Overexpression of ASNS might inhibit JNK phosphorylation to block c-Jun-associated apoptosis in resistant cells. We found that mPR binds to PDK-1 to induce Akt phosphorylation and promote cell survival. Resistant cells might exploit this process to escape doxorubicin-induced cell death. Moreover, GSTO-1 plays a role in stimulating the Akt-related pathway to promote cell survival in resistant cells. Identified proteins involved in drug-resistant networks are highlighted in red. Purple arrows represent doxorubicin-modulated proteins expressed by MES-SA cells, and blue arrows represent baseline resistances between MES-SA/Dx5 and MES-SA cells. (For interpretation of the references to color in this figure legend, the reader is referred to the web version of this article.)

peroxide, and oxygen to produce reactive oxygen species (ROS), leading to cell damage or even cell death [21–23]. Thus, chemotherapy-resistant cancer cells develop defense mechanisms, including overexpression of redox-modulated proteins to scavenge doxorubicin-induced ROS. In this study, we demonstrated the upregulation of peroxiredoxin 2 in MES-SA/Dx5 cells, with the implication that peroxiredoxin 2 reduces ROS levels and prevents ROS-induced cytotoxicity in resistant cells. Similarly, glutathione S-transferase omega-1 showed significant downregulation during doxorubicin treatment of MES-SA but not in MES-SA/Dx5 cells, implying that glutathione S-transferase omega-1 plays an anti-apoptotic role in cell resistance against doxorubicin toxicity in MES-SA/Dx5 cells. Bcl-2 may sequester calcineurin A and inhibit Fas/FasL-dependent apoptosis through de-phosphorylation of NEAT by calcineurin A [24]. This study demonstrated that calcineurin A

is significantly downregulated in MES-SA/Dx5, but not in MES-SA cells, suggesting that downregulation of calcineurin A inhibits doxorubicin-induced cell apoptosis by constitutively blocking the de-phosphorylation of NEAT in MES-SA/Dx5 cells.

Nucleophosmin (NPM1) was originally reported as a non-ribosomal nucleolar phosphoprotein that occurs at high levels in the granular regions of the nucleolus [25]; it is highly conserved in vertebrates and is widely distributed across different species [26]. NPM1 is a multifunctional protein associated with an array of biological and pathological processes. For example, nucleolar protein B23 can shuttle between the nucleus and cytoplasm during various stages of the cell cycle [27], and it may play a role as a molecular chaperone to prevent protein aggregation and thermal denaturation [28]. Thus, NPM1 may play an important role in protecting uterine cells from environmental stresses, such as doxorubicin attack. Additionally, the overexpression of NPM1 in resistant cells might also inhibit IRF-1 activity to decrease mitochondrial permeability and inhibit doxorubicin-induced programed cell death [29,30]. In accordance with our findings, NPM1 is upregulated in MES-SA/Dx5, but not in MES-SA cells. Additionally, comparison with MES-SA/Dx5 cells shows that NPM1 deregulates in MES-SA cells following treatment with doxorubicin.

Reticulocalbin-1 (RCN 1) is an endoplasmic reticulum-resident calcium-binding protein. Kuramitsu et al. used proteomic analysis to associate the increased expression of RCN 1 with the acquisition of gemcitabine drug resistance [31]. In our study, upregulation of RCN 1 was apparent in MES-SA/Dx5 cells, suggesting that its increased expression correlates with multiple drug resistance in cancer cells. To the best of our knowledge, this study is the first to report RCN 1 as a resistance marker for doxorubicin resistance.

Several key regulatory proteins mediate the interaction of heat shock proteins to block apoptosis. The intrinsic pathway of caspase-mediated apoptosis is stimulated by c-Jun kinase, resulting in the release of cytochrome c from the mitochondria, and the subsequent activation of a caspase cascade involving caspases 8 and 3, each of which is inhibited by heat shock cognate 71. Furthermore, heat shock cognate 71 interacts with Bcl-2 through Bag-1, allowing incorporation of the complex into the mitochondrial membrane to inhibit apoptosis [32]. Heat shock protein 27 inhibits the extrinsic apoptotic pathway through death receptors at caspase 9 [33,34]. In this study, heat shock cognate 71 and heat shock protein 27 were both downregulated in doxorubicin-treated MES-SA but not in MES-SA/Dx5 cells, implying that heat shock cognate 71 and heat shock protein 27 are essential for the development of doxorubicin resistance in uterine cancer, and are potential targets for resistance-related therapies.

Calumenin was strongly upregulated in our doxorubicin-resistant MES-SA/Dx5 cells. The protein inserts into the endoplasmic reticulum during regulation of cellular Ca^{2+} [35]; the release of the Ca^{2+} ion from the endoplasmic reticulum under stress conditions is a known mechanism for inducing apoptosis. Thus, researchers have proposed that calumenin is responsible for calcium sequestration, and that it blocks doxorubicin-induced apoptosis [36,37]. We found that calumenin levels were elevated in MES-SA/Dx5 cells, whereas its expression was downregulated in doxorubicin-treated MES-SA cells. This demonstrates that calumenin plays a role in the formation of doxorubicin resistance in uterine cancer, and is thus a potential target for resistance-related therapies.

In our proteomic analysis of doxorubicin resistance in uterine cancer, we selected 2 potential target proteins, mPR and ASNS, for further evaluation of their potential as therapeutic targets, because they each exhibited significant upregulation in resistant lines during proteomic analysis. A number of cancer cells overexpress mPR compared to normal cells, and thus, mPR is recognized as an important disease marker for cancer detection and cancer progression, and is a potential chemotherapeutic target [38,39]. The mPR protein is involved in the control of cancer cell proliferation and growth [40] through direct interactions between its cytochrome b5-binding domain and target proteins such as Insig-1 [41]. Recent studies report that mPR mediates progesterone's anti-apoptotic function [42] and induces Akt phosphorylation to promote cell survival [43]. However, there are no literature reports of the role of mPR in doxorubicin drug resistance in uterine cancer. The second target protein, ASNS, catalyzes cellular aspartate conversion to asparagine. Previous reports have indicated that overexpression of ASNS inhibits JNK phosphorylation to block c-Jun-associated apoptosis in pancreatic cancer cells, and proposed blocking the biosynthesis of ASNS as a practical strategy for pancreatic cancer therapy [44]. ASNS studies have tended to focus on the enzyme's role in leukemia. Inhibition of ASNS is an alternative approach to deprive malignant lymphocytes because these cells are highly reliant on asparagine; thus, ASNS inhibitors might offer a strategy for inhibiting protein biosynthesis in malignant lymphocytes. In agreement with our proteomic results, ASNS was overexpressed in resistant uterine cancer cells, and ASNS inhibitors used in leukemia therapy, such as adenylated sulfoximines, are therefore candidates for treating doxorubicin resistance. We found that knockdown of mPR or ASNS causes significantly reduced viability of MES-SA/Dx5 cells, but not MES-SA cells, suggesting the potential application of ASNS to the inhibition of doxorubicin resistance in uterine cancer therapy.

Conducting proteomic analysis using a large-scale 2D-DIGE system with MALDI-TOF/TOF MS was effective in the detection of uterine proteins with differential expression in uterine cancer cell lines that were sensitive or resistant to doxorubicin. Such proteins may be involved in chemotherapy resistance mechanisms. We grouped the proteins identified in this study, and proposed doxorubicin resistance mechanisms that may occur in MES-SA cells (Fig. 10). The identified upregulated proteins might serve as indicators for predicting the response of uterine cancer patients to treatment with doxorubicin or other drugs such as 5-fluorouracil. This study showed that ASNS and mPR proteins are useful in the alleviation of doxorubicin drug resistance. Further clinical research is needed to evaluate these 2 proteins' potential as therapeutic targets.

Supplementary data to this article can be found online at http://dx.doi.org/10.1016/j.ymgme.2012.07.025.

Declaration of competing interests

The authors confirm that there are no conflicts of interest.

Acknowledgement

This work was supported by NSC grant (99-2311-B-007-002, 100-2311-B-007-005 and 101-2311-B-007-011) from the National Science Council, Taiwan, NTHU and CGH grant (100N2723E1) from the National Tsing Hua University, NTHU Booster grant (99N2908E1) from the National Tsing Hua University, Toward Word-Class University project from National Tsing Hua University (100N2051E1) and VGHUST grant (99-P5-22) from the Veteran General Hospitals University System of Taiwan.

REFERENCES

[1] Lage H. An overview of cancer multidrug resistance: a still unsolved problem. Cell Mol Life Sci 2008;65:3145-67.
[2] Verma S, Dent S, Chow BJ, Rayson D, Safra T. Metastatic breast cancer: the role of pegylated liposomal doxorubicin after conventional anthracyclines. Cancer Treat Rev 2008;34: 391-406.
[3] Vatsyayan R, Chaudhary P, Lelsani PC, Singhal P, Awasthi YC, Awasthi S, et al. Role of RLIP76 in doxorubicin resistance in lung cancer (review). Int J Oncol 2009;34:1505-11.
[4] Green AE, Rose PG. Pegylated liposomal doxorubicin in ovarian cancer. Int J Nanomedicine 2006;1:229-39.
[5] Hui RC, Francis RE, Guest SK, Costa JR, Gomes AR, Myatt SS, et al. Doxorubicin activates FOXO3a to induce the expression of multidrug resistance gene ABCB1 (MDR1) in K562 leukemic cells. Mol Cancer Ther 2008;7:670-8.
[6] Harisi R, Dudas J, Nagy-Olah J, Timar F, Szendroi M, Jeney A. Extracellular matrix induces doxorubicin-resistance in human osteosarcoma cells by suppression of p53 function. Cancer Biol Ther 2007;6:1240-6.
[7] Ferreira MJ, Duarte N, Gyemant N, Radics R, Cherepnev G, Varga A, et al. Interaction between doxorubicin and the resistance modifier stilbene on multidrug resistant mouse lymphoma and human breast cancer cells. Anticancer Res 2006;26:3541-6.
[8] Song X, Liu X, Chi W, Liu Y, Wei L, Wang X, et al. Hypoxia-induced resistance to cisplatin and doxorubicin in non-small cell lung cancer is inhibited by silencing of HIF-1alpha gene. Cancer Chemother Pharmacol 2006;58: 776-84.
[9] Biing JT, Yang YF, Liu HS, Ye CT, Chao CF. The induction of multidrug resistance in human cervical carcinoma cell lines by estrogenic hormones. Proc Natl Sci Counc Repub China B 1994;18:64-70.
[10] Timms JF, Cramer R. Difference gel electrophoresis. Proteomics 2008;8:4886-97.
[11] Lai TC, Chou HC, Chen YW, Lee TR, Chan HT, Shen HH, et al. Secretomic and proteomic analysis of potential breast cancer markers by two-dimensional differential gel electrophoresis. J Proteome Res 2010;9:1302-22.
[12] Chou HC, Chen YW, Lee TR, Wu FS, Chan HT, Lyu PC, et al. Proteomics study of oxidative stress and Src kinase inhibition in H9C2 cardiomyocytes: a cell model of heart ischemia reperfusion injury and treatment. Free Radic Biol Med 2010;49:96–108.
[13] Wu CL, Chou HC, Cheng CS, Li JM, Lin ST, Chen YW, et al. Proteomic analysis of UVB-induced protein expression- and redox-dependent changes in skin fibroblasts using lysine- and cysteine-labeling two-dimensional difference gel electrophoresis. J Proteomics 2012;75:1991-2014.
[14] Harker WG, Sikic BI. Multidrug (pleiotropic) resistance in doxorubicin-selected variants of the human sarcoma cell line MES-SA. Cancer Res 1985;45:4091-6.
[15] Harker WG, MacKintosh FR, Sikic BI. Development and characterization of a human sarcoma cell line, MES-SA, sensitive to multiple drugs. Cancer Res 1983;43:4943-50.
[16] Noh DY, Ahn SJ, Lee RA, Kim SW, Park IA, Chae HZ. Overexpression of peroxiredoxin in human breast cancer. Anticancer Res 2001;21:2085-90.
[17] Torosyan Y, Simakova O, Naga S, Mezhevaya K, Leighton X, Diaz J, et al. Annexin-A7 protects normal prostate cells and induces distinct patterns of RB-associated cytotoxicity in androgen-sensitive and -resistant prostate cancer cells. Int J Cancer 2009;125:2528-39.
[18] Tu SH, Chang CC, Chen CS, Tam KW, Wang YJ, Lee CH, et al. Increased expression of enolase alpha in human breast cancer confers tamoxifen resistance in human breast cancer cells. Breast Cancer Res Treat 2010;121:539-53.
[19] Bonfils C, Bec N, Larroque C, Del Rio M, Gongora C, Pugniere M, et al. Cyclophilin A as negative regulator of apoptosis by sequestering cytochrome c. Biochem Biophys Res Commun 2010;393:325-30.
[20] Zhang D, Putti TC. Over-expression of ERp29 attenuates doxorubicin-induced cell apoptosis through up-regulation of Hsp27 in breast cancer cells. Exp Cell Res 2010;316:3522-31.
[21] Injac R, Strukelj B. Recent advances in protection against doxorubicin-induced toxicity. Technol Cancer Res Treat 2008;7:497-516.
[22] Kotamraju S, Kalivendi SV, Konorev E, Chitambar CR, Joseph J, Kalyanaraman B. Oxidant-induced iron signaling in Doxorubicin-mediated apoptosis. Methods Enzymol 2004;378:362-82.
[23] Taatjes DJ, Fenick DJ, Gaudiano G, Koch TH. A redox pathway leading to the alkylation of nucleic acids by doxorubicin and related anthracyclines: application to the design of antitumor drugs for resistant cancer. Curr Pharm Des 1998;4:203-18.
[24] Srivastava RK, Sasaki CY, Hardwick JM, Longo DL. Bcl-2-mediated drug resistance: inhibition of apoptosis by blocking nuclear factor of activated T lymphocytes (NFAT)-induced Fas ligand transcription. J Exp Med 1999;190: 253-65.
[25] Yung BY, Busch H, Chan PK. Translocation of nucleolar phosphoprotein B23 (37 kDa/pI 5.1) induced by selective inhibitors of ribosome synthesis. Biochim Biophys Acta 1985;826:167-73.
[26] Chang JH, Olson MO. Structure of the gene for rat nucleolar protein B23. J Biol Chem 1990;265:18227-33.
[27] Szebeni A, Herrera JE, Olson MO. Interaction of nucleolar protein B23 with peptides related to nuclear localization signals. Biochemistry 1995;34:8037-42.
[28] Szebeni A, Olson MO. Nucleolar protein B23 has molecular chaperone activities. Protein Sci 1999;8:905-12.
[29] Kondo T, Minamino N, Nagamura-Inoue T, Matsumoto M, Taniguchi T, Tanaka N. Identification and characterization of nucleophosmin/B23/numatrin which binds the anti-oncogenic transcription factor IRF-1 and manifests oncogenic activity. Oncogene 1997;15:1275-81.
[30] Lee HJ, Oh YK, Rhee M, Lim JY, Hwang JY, Park YS, et al. The role of STAT1/IRF-1 on synergistic ROS production and loss of mitochondrial transmembrane potential during hepatic cell death induced by LPS/d-GalN. J Mol Biol 2007;369:967-84.
[31] Kuramitsu Y, Taba K, Ryozawa S, Yoshida K, Zhang X, Tanaka T, et al. Identification of up- and down-regulated proteins in gemcitabine-resistant pancreatic cancer cells using two-dimensional gel electrophoresis and mass spectrometry. Anticancer Res 2010;30:3367-72.
[32] Takayama S, Krajewski S, Krajewska M, Kitada S, Zapata JM, Kochel K, et al. Expression and location of Hsp70/Hsc-binding

anti-apoptotic protein BAG-1 and its variants in normal tissues and tumor cell lines. Cancer Res 1998;58:3116-31.
[33] Hsu HS, Lin JH, Huang WC, Hsu TW, Su K, Chiou SH, et al. Chemoresistance of lung cancer stemlike cells depends on activation of Hsp27. Cancer 2011;117:1516-28.
[34] Concannon CG, Orrenius S, Samali A. Hsp27 inhibits cytochrome c-mediated caspase activation by sequestering both pro-caspase-3 and cytochrome c. Gene Expr 2001;9: 195-201.
[35] Cho JH, Song HO, Singaravelu G, Sung H, Oh WC, Kwon S, et al. Pleiotropic roles of calumenin (calu-1), a calcium-binding ER luminal protein, in *Caenorhabditis elegans*. FEBS Lett 2009;583:3050-6.
[36] Castagna A, Antonioli P, Astner H, Hamdan M, Righetti SC, Perego P, et al. A proteomic approach to cisplatin resistance in the cervix squamous cell carcinoma cell line A431. Proteomics 2004;4:3246-67.
[37] Wu W, Tang X, Hu W, Lotan R, Hong WK, Mao L. Identification and validation of metastasis-associated proteins in head and neck cancer cell lines by two-dimensional electrophoresis and mass spectrometry. Clin Exp Metastasis 2002;19:319-26.
[38] Xu J, Zeng C, Chu W, Pan F, Rothfuss JM, Zhang F, et al. Identification of the PGRMC1 protein complex as the putative sigma-2 receptor binding site. Nat Commun 2011;2:380.
[39] Cahill MA. Progesterone receptor membrane component 1: an integrative review. J Steroid Biochem Mol Biol 2007;105:16-36.
[40] Neubauer H, Adam G, Seeger H, Mueck AO, Solomayer E, Wallwiener D, et al. Membrane-initiated effects of progesterone on proliferation and activation of VEGF in breast cancer cells. Climacteric 2009;12:230-9.
[41] Yang T, Espenshade PJ, Wright ME, Yabe D, Gong Y, Aebersold R, et al. Crucial step in cholesterol homeostasis: sterols promote binding of SCAP to INSIG-1, a membrane protein that facilitates retention of SREBPs in ER. Cell 2002;110:489-500.
[42] Peluso JJ, Pappalardo A, Losel R, Wehling M. Progesterone membrane receptor component 1 expression in the immature rat ovary and its role in mediating progesterone's antiapoptotic action. Endocrinology 2006;147:3133-40.
[43] Neubauer H, Clare SE, Wozny W, Schwall GP, Poznanovic S, Stegmann W, et al. Breast cancer proteomics reveals correlation between estrogen receptor status and differential phosphorylation of PGRMC1. Breast Cancer Res 2008;10:R85.
[44] Cui H, Darmanin S, Natsuisaka M, Kondo T, Asaka M, Shindoh M, et al. Enhanced expression of asparagine synthetase under glucose-deprived conditions protects pancreatic cancer cells from apoptosis induced by glucose deprivation and cisplatin. Cancer Res 2007;67:3345-55.